MANUAL OF THE E-PHYSICS

(Mellor - Yamada turbulence closure model,
Monin - Obukhov surface layer processes,
and land/sea conditions)

by

K. Miyakoda and J. Sirutis

Geophysical Fluid Dynamics Laboratory/NOAA

Princeton University, P.O. Box 308

Princeton, New Jersey 08540 USA

Contents

Preface

Figure 1 illustrates the general concept of the so-called "physics" in a general circulation model (GCM). The solar radiation is the whole source of energy given to the atmosphere. It first penetrates into the earth's surface. The energy is then released to the atmosphere in the form of evaporation for a large portion and in the form of sensible heat transfer for the rest of the portion. The moisture thus produced condenses, releasing a great deal of latent heat. This subject, however, will be discussed separately as the F-physics.

Fig. 1

Near the earth's surface, there is a boundary layer, which is the transitional zone from solid or liquid surfaces to gaseous media. The thickness of the layer is $0 \sim 1.5$ km over land and $200 \sim 700$ m over ocean. This layer is referred to as the planetary boundary layer (PBL), which is formed and controlled mostly by surface heating. In fact, the depth over land varies considerably with the local time (figure 2). Wind speed in the PBL decreases with approaching the earth's surface, simply because of the geometric constraint. If one emphasizes the aspect of vertical profile of wind speed, considering the effect of the earth's rotation, the layer can be considered as the Ekman layer, but the thermal effect dominates the PBL process in reality.

Fig. 2

The PBL is full of turbulent energy, because the turbulence is produced due to the buoyancy associated with the surface heating and partially due to the mechanical energy associated with the vertical wind shear. As a result of turbulent mixing, the heat and moisture are well mixed in the entire PBL. Observations reveal that potential temperature and the specific humidity distribute in almost constant with height. For this reason the PBL is also referred to as the mixed layer.

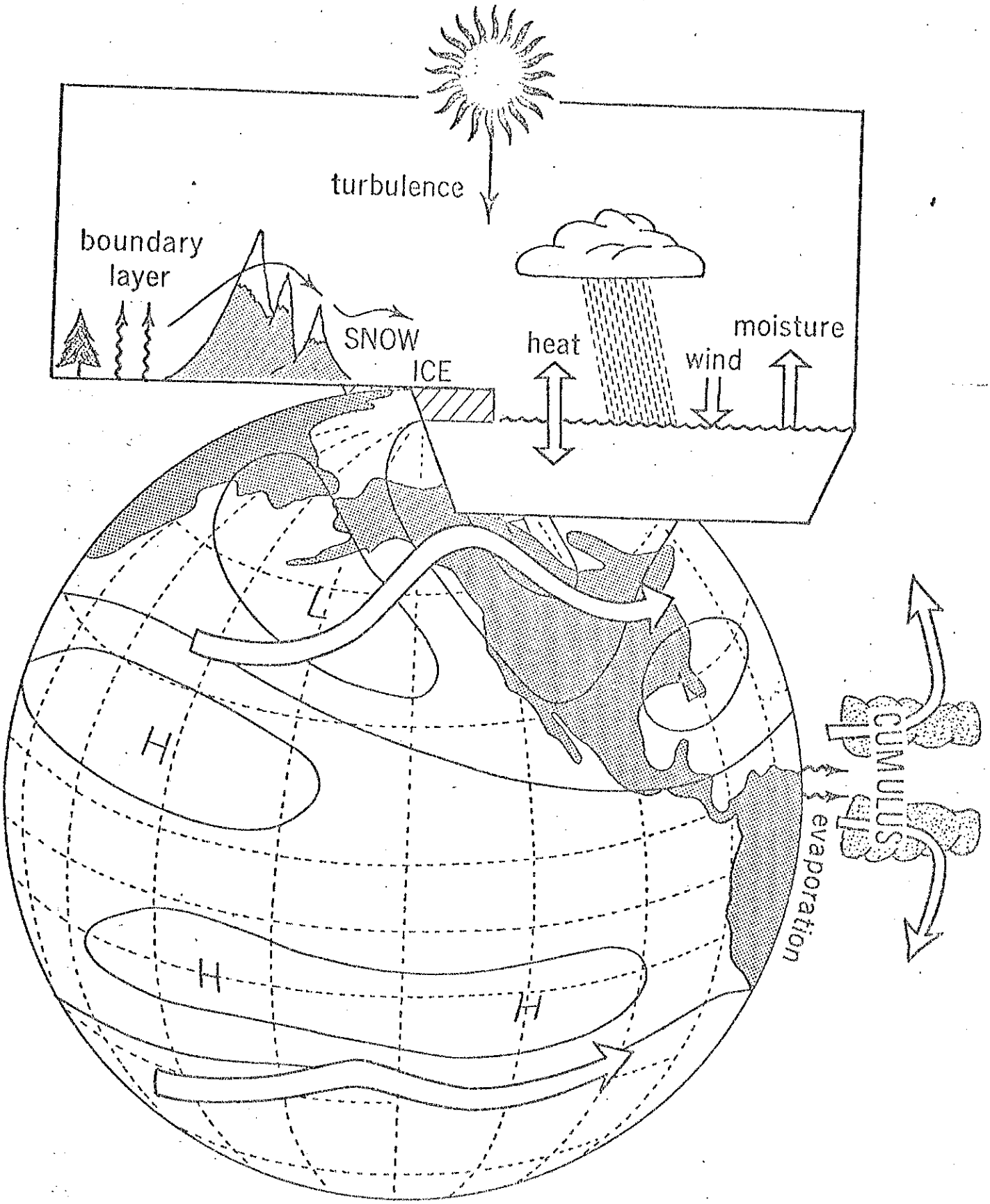

Fig. 1 Schematic picture of a general circulation model (GCM) and its physics. The physics is indicated in the upper box and the cumulus clouds at the equatorial zone in the lower globe.

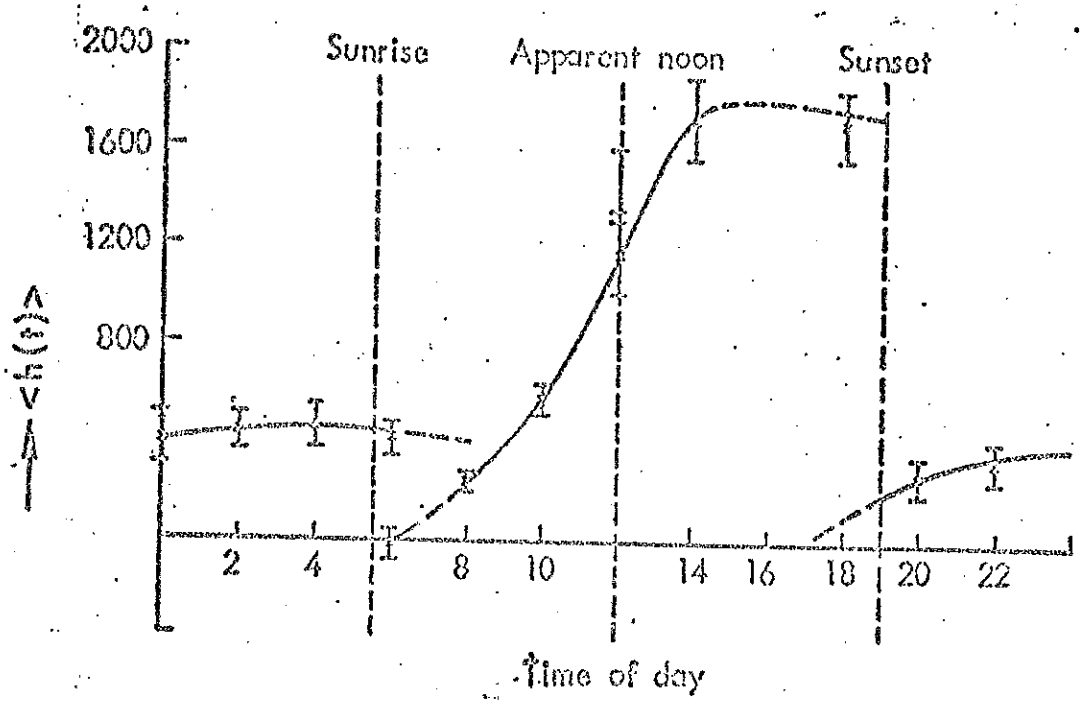

Fig. 2 The mean boundary-layer thickness, $\langle h(t) \rangle$, deduced for the O'Neill data and plotted with standard errors in mean solar time (after Carson, 1973).

Inside the PBL (figure 3) the diurnal variability is pronounced; a nocturnal jet is generated; the moisture and sensible heat are vigorously advected in the horizontal; the snow is deposited; and the hydrological process including the vegetation takes place. An understanding of these events and phenomena is important for determining the so-called external (abnormal) forcings that influence substantially the atmospheric state.

Fig. 3

The turbulence exists not only in the PBL but also in the free atmosphere. At high altitude, say at 100 mb, a considerable intensity of turbulence is often found, which is known as the clear air turbulence. It is likely that dissipation of kinetic energy takes place at the jet stream level in addition to the major dissipation in the PBL.

The E-physics of the GFDL GCM treats the turbulent processes in the PBL as well as in the free atmosphere, if the grid resolution is sufficiently fine. The E-physics includes the turbulence closure scheme, the treatment of surface boundary layer, the heat balance at the earth's surface, and the soil heat conduction. This model is, therefore, capable of reproducing the nocturnal jet, the overall diurnal variability of the PBL, the clear-air turbulence, mimicing snow deposits, and also a certain degree of land surface hydrology, through which the content of soil moisture is determined.

It is our view that the treatment of the subgrid-scale processes included in the E-physics is essential in calculating proper features of the meteorological and hydrological conditions at or next to the earth's surface and the diffusive character of momentum, heat and moisture in the PBL as well as in the free atmosphere. These conditions in turn exert a substantial impact on determining the intensity of westerly jet, its meandering, and accordingly the teleconnection characteristics of general circulation (see figure 1).

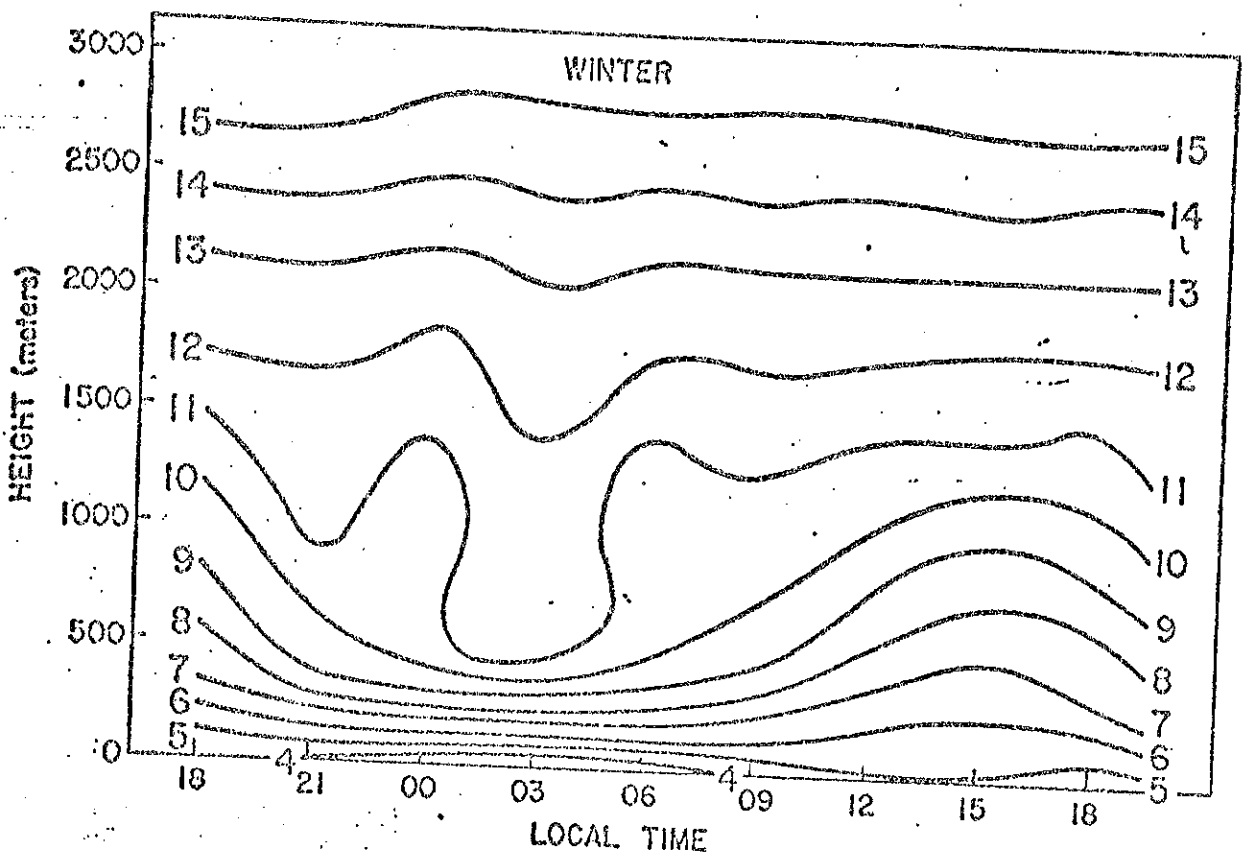

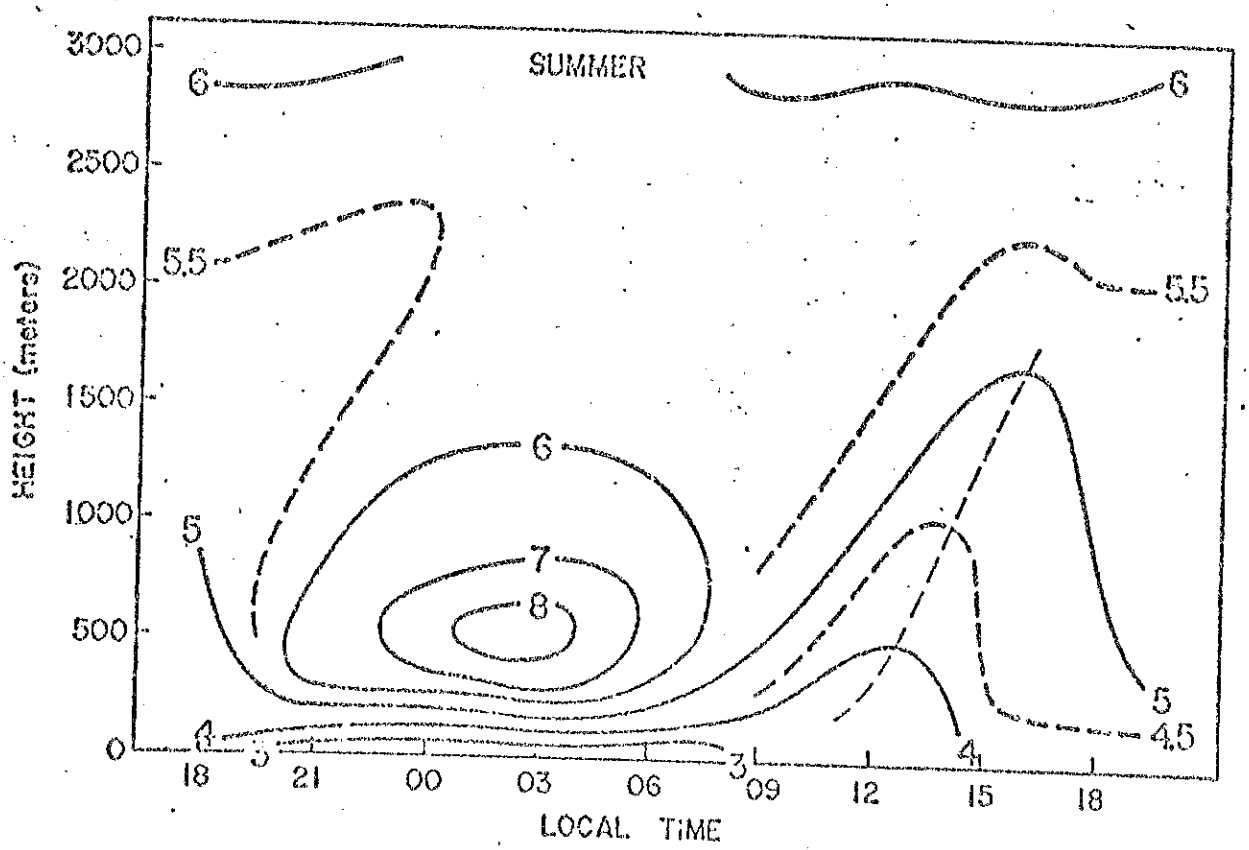

Fig. 3 Diurnal variation of the wind speed as a function of height. Values are based on data from Jackson, Mississippi; Shreveport, Louisiana; and Montgomery, Alabama (after Hoxit, 1973).

1. Introduction

There are three major items in the E-physics, i.e., the turbulence closure scheme, the Monin-Obukhov similarity scheme, and the land/sea surface processes.

The historical development of the turbulence closure theory is not our concern here. The particular model described in this manual is the second-order closure scheme of Mellor-Yamada's (1974) at the hierarchy level 2.5, in which the equation of turbulent kinetic energy is time-dependent, but the equation of the second-moment of thermal fluctuation is stationary. There are six or seven parameters which should be specified based on empirical evidences. Actually they have been determined based on neutral stratification in laboratory experiments. It is one of the major unique features that these parameters are commonly used for any media, such as the ocean or the Jupiter atmosphere without any consideration. Then our strategy is that, once these parameters are decided, they should not be changed arbitrarily, and other ad hoc treatments are not applied. The PBL processes are adequately represented by this scheme. The sharp transition of the thermal profile at the top of the PBL could be reproduced, though the simulated jump is not so conspicuous as in the model of hierarchy level 3. One of the merits in the level 2.5 model is that the turbulence is spatially diffused both in the vertical and the horizontal from the turbulence generating area to the stable area. As a result, the moisture in the PBL, for example, is adequately distributed above the PBL (say up to 3 km), whereas in the level 2 model, the diffusion is confined in the unstable region (Richardson number is less than 0.21) and therefore, limited to the PBL except for eviction through clouds.

The level 2.5 model would be capable of simulating the nocturnal jet (see section 8), the clear-air turbulence, if the grid resolution is adequate, and the turbulent transport process in the surface layer.

However, in order to simulate the fluxes close to the earth's surface, a fine vertical resolution is required for a numerical model. For reasons of economy, a bulk method is employed, i.e., processes based on the Monin-Obukhov similarity theory. They are (almost) consistent in physics to the turbulence closure level 2.5 scheme.

The third aspect of E-physics is the surface processes, which consist of the retention of moisture in soil, the runoff, the snow melt and snow deposit, the evapotranspiration, the soil heat conduction, the heat balance at the surface, the surface albedo, and sea ice heat conduction.

2. Grid-box Mean

It is inevitable that a GCM uses a finite grid length instead of a continuous coordinate in specifying the fluid dynamical equations. Associated with this space descritization, variables and equations are divided into the grid scale averages and their deviations. The effects arising from non-linear coupling of these deviations are the sub-grid scale (SGS) processes.

In practice, however, the mathematical treatment of the grid-box average is too complicated and awkward to handle. So, the ensemble mean and its deviation are normally taken, and the resulting formulas are then switched to the spatial mean and its deviations, ignoring additional terms (Leonard's term, for example; see Leonard, 1973; Clarke et al, 1979).

$$u = \overline{u} + u'$$

$$v = \overline{v} + v'$$

The bar is the ensemble mean, and the prime is its departure. In this manual, the second-moment $\overline{u'v'}$ is hereafter written as $\overline{uv}$ for simplicity, by dropping the prime notations. The bar notation for the first moment is often dropped too. As is readily conceived, the character of the SGS processes is very similar to that of turbulence, thus enabling us to utilize the wealth of knowledge on turbulence accumulated in the past.

2.1 Basic equations

The dependent variables of grid-resolvable scale in the E-physics version of GCM are: u, v, θ, q and b^2, where q is the mixing ratio of water vapor and $1/2b^2$ is the turbulent kinetic energy, $1/2\ b^2=1/2(\overline{u^2}+\overline{v^2}+\overline{w^2})$. The equations are normally written on the pressure coordinate (or the

σ -coordinate). However, the SGS terms will be expressed on z-coordinate.

$$\frac{du}{dt} - fv + \frac{1}{\rho}\frac{\partial p}{\partial x}$$

$$= \frac{1}{\rho}\left(\frac{\partial \tau_{xx}}{\partial x} + \frac{\partial \tau_{xy}}{\partial y} + \frac{\partial \tau_{xz}}{\partial z}\right) \quad (2.1)$$

$$\frac{dv}{dt} + fu + \frac{1}{\rho}\frac{\partial p}{\partial y}$$

$$= \frac{1}{\rho}\left(\frac{\partial \tau_{yx}}{\partial x} + \frac{\partial \tau_{yy}}{\partial y} + \frac{\partial \tau_{yz}}{\partial z}\right) \quad (2.2)$$

$$\frac{d\theta}{dt} = \frac{1}{\rho}\left(\frac{\partial \tau_{\theta x}}{\partial x} + \frac{\partial \tau_{\theta y}}{\partial y} + \frac{\partial \tau_{\theta z}}{\partial z}\right)$$

$$+ Q_R + \gamma(c - e) \quad (2.3)$$

$$\frac{dq}{dt} = \frac{1}{\rho}\left(\frac{\partial \tau_{qx}}{\partial x} + \frac{\partial \tau_{qy}}{\partial y} + \frac{\partial \tau_{qz}}{\partial z}\right)$$

$$-(c - e) \quad (2.4)$$

$$\frac{d\,b^2/2}{dt} = \frac{\partial}{\partial z}\left(\frac{5}{3} l\, b^2 \frac{\partial b^2/2}{\partial z}\right)$$

$$- \overline{w'w'}\frac{\partial V}{\partial z} + \frac{g}{\theta_0}\overline{w'\theta_v'} - \frac{b^3}{\Lambda} \quad (2.5)$$

where $\gamma \equiv \frac{L \cdot \theta_o}{C_p \cdot T_{oo}}$, θ_o is the horizontal mean of θ, T_{oo} is the reference temperature, L is the latent heat, c and e are the rates of condensation and evaporation, ℓ and Λ are the turbulent scale length, g is the acceleration of gravity, and θ_v is the virtual potential temperature.

τ_{xx}, τ_{xy}.....τ_{yz} are the Reynolds stress terms, i.e.,

$$\begin{pmatrix} \tau_{xx} & \tau_{xy} & \tau_{xz} \\ \tau_{yx} & \tau_{yy} & \tau_{yz} \end{pmatrix} = \begin{pmatrix} -\rho\overline{u'u'} & -\rho\overline{uv} & -\rho\overline{uw} \\ -\rho\overline{vu} & -\rho\overline{v'v'} & -\rho\overline{vw} \end{pmatrix}$$

and the covariances of θ or q and momentum are:

$$\begin{pmatrix} \tau_{\theta x} & \tau_{\theta y} & \tau_{\theta z} \\ \tau_{qx} & \tau_{qy} & \tau_{qz} \end{pmatrix} = \begin{pmatrix} -\rho\overline{\theta u} & -\rho\overline{\theta v} & -\rho\overline{\theta w} \\ -\rho\overline{qu} & -\rho\overline{qv} & -\rho\overline{qw} \end{pmatrix}$$

2.2 Lateral diffusion

The formulation of eddy viscosity is made using an assumption on the rate of strain of fluid analogous to an elastic media (Smagorinsky, 1963). The shear stress is assumed to be linearly proportional to the rate of deformation. Let tensor τ_{ij} represent τ_{xx}, τ_{xy}.....Then

$$\tau_{ij} = K_M \cdot D_{ij} \qquad (2.8)$$

where K_M is a parameter, and D_{ij} is the rate of deformation. So for the 2-dimensional case

$$\left[D_{ij}\right] = \begin{bmatrix} D_{xx} & D_{xy} \\ D_{yx} & D_{yy} \end{bmatrix} = \begin{pmatrix} 2\frac{\partial u}{\partial x} - \nabla\cdot v & \frac{\partial u}{\partial y} + \frac{\partial v}{\partial x} \\ \frac{\partial v}{\partial x} + \frac{\partial u}{\partial y} & 2\frac{\partial v}{\partial y} - \nabla\cdot v \end{pmatrix}$$

$$= \begin{pmatrix} \frac{\partial u}{\partial x} - \frac{\partial v}{\partial y} & \frac{\partial u}{\partial y} + \frac{\partial v}{\partial x} \\ \frac{\partial v}{\partial x} + \frac{\partial u}{\partial y} & \frac{\partial v}{\partial y} - \frac{\partial u}{\partial x} \end{pmatrix} = \begin{pmatrix} D_T & D_S \\ D_S & -D_T \end{pmatrix} \qquad (2.9)$$

Later we will use the notations of D_T and D_S.

Similarly

$$\frac{1}{\rho}\begin{pmatrix} \tau_{ox} & \tau_{oy} \\ \tau_{qx} & \tau_{qy} \end{pmatrix} = K_H \begin{pmatrix} \frac{\partial \theta}{\partial x} & \frac{\partial \theta}{\partial y} \\ \frac{\partial q}{\partial x} & \frac{\partial q}{\partial y} \end{pmatrix} \qquad (2.10)$$

non-linear viscosity

Smagorinsky (1963) derived the formula of K_M to be consistent to the Kolmogoroff theory on the turbulence scale, i.e., E (wave energy) $\propto L^{5/3}$, L being the length scale. The formula is,

$$K_M = \text{const.}\ \Delta^2 |D| \qquad (2.11)$$

where Δ is the grid size of a GCM, and

$$D^2 = D_{xx}^2 + D_{xy}^2 + D_{yx}^2 + D_{yy}^2$$
$$= 2\,(D_S^2 + D_T^2)$$

As will be discussed later

$$K_M = \frac{5}{2} K_M \qquad (2.11')$$

The value for the constant in (2.11) will be explained in setion 3.4.

If a function of $|D|$ is a variable in space, K_M and K_H are non-linear. This situation is similar to that in the PBL; the vertical eddy viscosity coefficient is proportional to $|\frac{\partial V}{\partial z}|$. In other words, if the latter is true (dependent on the local value of $|\frac{\partial V}{\partial z}|$), K_M and K_H should be non-linear.

Smagorinsky used the form

$$K_M = \left(\frac{c \cdot \Delta}{\sqrt{2}}\right)^2 \cdot |D|$$
$$= \alpha \cdot |D| \qquad (2.12)$$

where c = 0.14 (see later).

Then the equations are:

$$\frac{du}{dt} = \text{- - - - - - -} + \frac{\partial}{\partial x}\left(\alpha\,|D|\,D_T\right) + \frac{\partial}{\partial y}\left(\alpha\,|D|\cdot D_S\right) \qquad (2.13)$$

$$\frac{dv}{dt} = \text{-------} + \frac{\partial}{\partial x}\left(\alpha |D| \cdot D_S\right) - \frac{\partial}{\partial y}\left(\alpha |D| \cdot D_T\right) \quad (2.14)$$

$$\frac{d\theta}{dt} = \text{-------} + \frac{\partial}{\partial x}\left(\alpha' |D| \frac{\partial \theta}{\partial x}\right) + \frac{\partial}{\partial y}\left(\alpha' |D| \frac{\partial \theta}{\partial y}\right)$$

$$\alpha' = \frac{5}{7}\alpha \quad (2.15)$$

Note that, as will be discussed in section 3.4, these non-linear viscosity can be derived from the turbulence closure theory (Lilly, 1967).

On the other hand, if $|D|$ is constant in space, $K_M = K$ is constant. The equations are written simply as

$$\frac{du}{dt} = \text{------} + K \nabla^2 u \quad (2.16)$$

$$\frac{dv}{dt} = \text{------} + K \nabla^2 v \quad (2.16')$$

$$\frac{d\theta}{dt} = \text{------} + \frac{5}{2} K \nabla^2 \theta \quad (2.16'')$$

where

$$K = \beta \cdot \Delta^{4/3} \quad (2.17)$$

and the constant β is

$$\beta = \frac{c^2}{2} \frac{\langle |D| \rangle}{\Delta^{3/2}} \quad (2.18)$$

$<|D|>$ being the ensemble mean of $|D|$ in the grid of Δ.

Recently the del-four diffusion, ∇^4 has been used; this is linear and yet the tendency of the non-linear viscosity is presumably included. So

$$\frac{du}{dt} = \text{-----} + \mu \nabla^4 u \tag{2.19}$$

$$\frac{dv}{dt} = \text{-----} + \mu \nabla^4 v \tag{2.19'}$$

$$\frac{d\theta}{dt} = \text{-----} + \frac{5}{2} \mu \nabla^4 \theta \tag{2.19''}$$

where

$$\mu = \beta' \Delta^{10/3} \tag{2.20}$$

and

$$\beta' = \frac{c^2}{2} \frac{<|D|>}{\Delta^{4/3}} \tag{2.21}$$

The Kolmogoroff theory concerns the three-dimensional turblence. In the case of GCM, however, the range in which the grid discritization falls is the two-dimensional turbulence inertia domain, in which enstrophy cascade is constant with wavenumber. This implies that E (wave energy) $\propto L$ instead of $L^{5/3}$. In this connection, Leith (1969) postulated that

$$K_M = \text{const.}\ \Delta^3 |\nabla \zeta| ,$$

where ζ is the relative vorticity.

However, there are only few papers that report successful tests with this formulation (Yamagishi, 1980, const=1.25).

3. Turbulence Closure Model

3.1 Philosophy of second-order closure model

There are several principles for the architecture of an adequate GCM, particularly for the parameterization of SGS processes. The parameterization should meet certain standards for the accuracy, the simplicity, the versatility, the robustness, the computer adaptability, the historical consistency, and perhaps the elegance. A mechanistic model is not always suited for this principle, because this type of model is developed for an explanation of mechanism. The mechanistic model tends to lack in the generality; the mixed layer model is one of the examples.

The turbulence closure model has a long historical background, has mathematical preciseness, the simplicity, and has the versatility. Mellor and Yamada (1974) have clarified the hierarchial levels of the second-order closure model by making a scale analysis. The particular scheme employed in this manual is closed by Rotta's energy redistribution hypothesis and the Kolmogoroff's isotropic turbulence dissipation hypothesis.

The level 2 model is sufficiently simple, because the scheme consists of the exact same forms of eddy viscosity, which are functions of Richardson number. As was mentioned earlier, however, the diffusion operates only in the unstable region, and outside of it no diffusion is allowed to exist. As a result, the diffusivity varies abruptly in space; this is unrealistic and unfavorable. It is often the case in the GCM output that a model atmosphere is too dry above the PBL. The level 3 model consists of a number of non-steady equations of turbulent variances and covariances, which can correct the above deficiency. But this model requires a considerable computational burden, treating more equations of the grid-

resolvable variables.

A compromise is to introduce a level 2.5 model, which includes the non-steady equation, Only for $\partial b^2/\partial t$, but all other equations exclude time-derivatives and diffusion terms. Consequently the scheme is considerably simplified; the turbulence transfers are all expressed by algebraic equations. The equation of $\partial\theta^2/\partial t$ is steady. As a result, a jump of θ_v at the top of PBL is not sharp, and the downward heat flux $\overline{w\theta}$ at the top of PBL is not strong. These drawbacks are the penalty one has to pay due to the simplification.

3.2 The equations of level 2.5 model

The equations of Mellor (1973) and Deardorff (1973a,b) are very similar except that, the characteristic parameters for the closure assumptions are different. Namely the turbulence scale length, ℓ, is used in Mellor (subsequently referred to M), whereas the grid size, Δ, is used in Deardorff (subsequently referred to D).

For example, the term of the pressure-velocity gradient correlations which are called "energy redistribution terms" are parameterized by Rotta's hypothesis but in different ways.

In the following, using the tensor notation u_j, u_j, u_k, two versions are shown, i.e.; first by M and second by D.

$$\overline{\frac{p}{\rho}\left(\frac{\partial u_i}{\partial x_j}+\frac{\partial u_j}{\partial x_i}\right)} =$$

$$\begin{cases} -\dfrac{q}{3\ell_1}\left(\overline{u_i u_j}-\dfrac{1}{3}\delta_{ij}q^2\right)+C\cdot q^2\left(\dfrac{\partial u_i}{\partial x_j}+\dfrac{\partial u_j}{\partial x_i}\right), \\ -\dfrac{C_m\cdot q}{2^{1/2}\Delta}\left(\overline{u_i u_j}-\dfrac{1}{3}\delta_{ij}q^2\right)+\dfrac{1}{5}q^2\left(\dfrac{\partial u_i}{\partial x_j}+\dfrac{\partial u_j}{\partial x_i}\right) \end{cases} \quad (3.1)$$

where p is the pressure, ℓ, is a scale length, c and c_m are constants. The viscous dissipation is expressed, based on Kolmogoroff's hypothesis, i.e.,

$$\nu \overline{\frac{\partial u_i}{\partial x_k} \frac{\partial u_j}{\partial x_k}} = \begin{cases} \dfrac{b^3}{\Lambda_1} \\ C_E \dfrac{b^3}{2^{3/2}\Delta} \end{cases}, \tag{3.2}$$

where ν is the molecular viscosity, Λ_1 is a scale length, and C_E is a constnt. The triple correlation is written as

$$\overline{u_i u_j u_k} = \begin{cases} -\frac{5}{3} b \lambda_1 \left(\frac{\partial \overline{u_i u_j}}{\partial x_k} + \frac{\partial \overline{u_i u_k}}{\partial x_j} + \frac{\partial \overline{u_j u_k}}{\partial x_i} \right), \\ -\frac{5}{3} \frac{C_{3m}}{2^{1/2}} \Delta \cdot b \left(\quad " \quad " \quad " \right) \end{cases} \tag{3.3}$$

where λ_1 is a scale length and C_{3m} is a constant. Thus the equation of turbulent kinetic energy is written by M and D, respectively, as

$$\frac{d\, b^2/2}{dt} = \begin{cases} \frac{\partial}{\partial z}\left(\ell b \frac{5}{3} \frac{\partial b^2/2}{\partial z} \right) \\ -\overline{vw} \frac{\partial v}{\partial z} + \frac{g}{\theta_0} \overline{w\theta_v} - \frac{b^3}{\Lambda_1}, \end{cases} \tag{3.4}$$

$$\left\{ \frac{\partial}{\partial z}\left(\frac{5}{3} \frac{C_{3m}}{2^{1/2}} \Delta \cdot b \frac{\partial b^2/2}{\partial z} \right) - \frac{1}{2} A_{ke} D_{ke} + \frac{g}{\theta_0} \overline{w\theta_v} - \frac{C_E}{2^{3/2}} \frac{b^3}{\Delta} \right. \tag{3.4'}$$

where

$$A_{ij} = \overline{u_i u_j} - \frac{1}{3} \delta_{ij} b^2 \tag{3.5}$$

$$D_{ij} = \frac{\partial u_i}{\partial x_j} + \frac{\partial u_j}{\partial x_i}$$

The terms on the right hand side of eqs. (4) represent the diffusion, the mechanical work due to wind shear, the work done by buoyancy, and the dissipation.

The vertical boundary condition for eq. (3.4) or (3.4') is

$$b^2 = B_1^{2/3} V_*^2 \qquad \text{at} \quad z = z_0 \tag{3.6}$$

z_0 and V_* being the roughness length and the friction velocity defined later in eq. (4.8), B_1=15, which will be explained in eq. (3.14).

Other equations of the second-moment of turbulence are assumed to be stationary and they are written by M and D, respectively, below.

$\frac{\partial \overline{u_i u_j}}{\partial t}$:

$$\left\{ \begin{aligned} 0 = {} & \frac{b}{3l_1}\left(\overline{u_i u_j} - \frac{1}{3}\delta_{ij}\, b^2\right) \\ & + C_1 \cdot b^2\left(\frac{\partial u_j}{\partial x_i} + \frac{\partial u_i}{\partial x_j}\right) - \frac{2}{3}\frac{b^2}{\Lambda_1}\delta_{ij} \\ & - \overline{u_i u_k}\frac{\partial u_j}{\partial x_k} - \overline{u_j u_k}\frac{\partial u_i}{\partial x_k} - 2\frac{g}{\theta_0}\overline{w\theta_v}\,, \end{aligned} \right. \tag{3.7}$$

$$0 = \frac{2}{15} b^2 D_{ij} - \frac{1}{3}\delta_{ij} \cdot A_{ik\ell} D_{k\ell} + \frac{C_m}{2^{1/2}}\frac{b}{\Delta} A_{ij} \tag{3.7'}$$
$$+ A_{ik}\frac{\partial u_j}{\partial x_k} + A_{jk}\frac{\partial u_i}{\partial x_k}$$
$$- \frac{g}{\theta_0}\left(\delta_{i3}\overline{u_j\theta} + \delta_{j3}\overline{u_i\theta} - \frac{2}{3}\delta_{ij}\cdot\overline{w\theta_v}\right)$$

$\frac{\partial \overline{u_i\theta}}{\partial t}$:

$$\left\{ \begin{aligned} 0 = {} & - \overline{u_i u_j}\frac{\partial \theta}{\partial x_j} - \overline{u_j\theta}\frac{\partial u_i}{\partial x_j} \\ & - \frac{b}{3l_2}\overline{u_i\theta} - \frac{g}{\theta_0}\overline{\theta\theta_v}\,, \end{aligned} \right. \tag{3.8}$$

$$\left\{ \begin{aligned} 0 = {} & - A_{ij}\frac{\partial \theta}{\partial x_j} - \overline{u_j\theta}\frac{\partial u_i}{\partial x_j} - \frac{1}{3} b^2 \frac{\partial \theta}{\partial x_i} \\ & - C_s \frac{b}{2^{1/2}\Delta}\overline{u_i\theta} + \frac{2}{3}\delta_{i3}\frac{g}{\theta_0}\overline{\theta^2} \end{aligned} \right. \tag{3.8'}$$

$\frac{\partial \theta^2}{\partial t}$:

$$\begin{cases} \dot{\theta} = -\overline{u_k \theta}\,\frac{\partial \theta}{\partial x_k} - \frac{b}{\Lambda_2}\overline{\theta^2} & (3.9) \\ 0 = -\overline{u_k \theta}\,\frac{\partial \theta}{\partial x_k} - c_0\,\frac{b}{2^{3/2}\Delta}\,\overline{\theta^2} & (3.9') \end{cases}$$

3.3 Eddy viscosity formulas

The manipulation of eq. (3.7), (3.8) and (3.9) for various i, j, k leads to algebraic equations. The results are summarized by the two equations as follows.

$$-\left(\overline{uw},\ \overline{vw}\right) = K_M\left(\frac{\partial u}{\partial z},\ \frac{\partial v}{\partial z}\right) \qquad (3.10)$$

$$-\left(\overline{\theta w},\ \overline{\theta w}\right) = K_H\left(\frac{\partial \theta}{\partial z},\ \frac{\partial \theta}{\partial z}\right) \qquad (3.11)$$

where

$$\begin{aligned} K_M = l_1 \Big[& (1-3c)b^5 + 3l_2\{(\Lambda_2 - 3l_2)b^3 \\ & - 3(4l_2 + \Lambda_2)c\,b^3\}\frac{g}{\theta_0}\frac{\partial \theta}{\partial z}\Big]\ \frac{\varepsilon}{\Delta} \\ & \Big[b^4 + 6l_1^2 b^2\left|\frac{\partial V}{\partial z}\right|^2 + 3l_1 l_2 \frac{g}{\theta_0}\frac{\partial \theta}{\partial z} \times \\ & \times\Big\{6l_1(\Lambda_1 - 3l_2)\left|\frac{\partial V}{\partial z}\right|^2 + \left(7 + \frac{\Lambda_2}{l_1}\right)b^2 \\ & + 9l_2(4l_1 + \Lambda_2)\frac{g}{\theta_0}\frac{\partial \theta}{\partial z}\Big\}\Big] \end{aligned} \qquad (3.12)$$

$$K_H = l_2\left[q^3 - 6 l_1 K_M \left|\frac{\partial V}{\partial z}\right|^2\right]^{\frac{1}{2}}$$

$$\left[q^2 + 3 l_2 (4 l_1 + \Lambda_2) \frac{g}{\theta_0}\frac{\partial \theta}{\partial z}\right] \qquad (3.13)$$

The numerical values of the constants are given basd on laboratory experiments (Deardorff, 1973; Mellor, 1973) as follows

(M)

$$l_1 = A_1 \cdot l \ , \quad l_2 = A_2 l$$
$$\Lambda_1 = B_1 \cdot l \ , \quad \Lambda_2 = B_2 l$$
$$\lambda_1 = \lambda_2 = \lambda_3 = 0.23\, l$$
$$(A_1, A_2, B_1, B_2, C) = (0.78, 0.78, 15, 8, 0.056) \qquad (3.14)$$

(D)

$$(C_m, C_s, C_E, C_0) = (4.13, 4.13, 0.70, 0.58)$$
$$(C_{3m}, C_{30}) = (0.2, 0.2) \qquad (3.15)$$

$$\frac{1}{\theta_0} = 0.00367 \qquad (3.16)$$

Mellor and Yamada (1982) reviewed the more recent data and gave:

$$(A_1, A_2, B_1, B_2, C) = (0.92, 0.74, 16.6, 10.1, 0.08) \qquad (3.17)$$

(See also Yamada and Mellor, 1979).

3.4 Turbulent length scale

The master length scale, l, has to be specified. Two versions are in current use.

Version I

This version is based on Blackadar's (1962) method. The formula combines two properties, i.e., $\ell \sim k_0 Z$ in the lowest level (k_0, Karman constant) and ℓ approaching to ℓ_0 at $z \to \infty$. Thus

$$\ell = \frac{k_0 \cdot z}{1 + \frac{k_0 z}{\ell_0}} \qquad (3.22)$$

where

$$\ell_0 = 0.10 \times \frac{\int_0^z b\, z\, \rho\, dz}{\int_0^z b\, \rho\, dz} \qquad (3.23)$$

This version has been used in this manual (see Miyakoda and Sirutis, 1977).

Version II

Mellor and Herring (1973) and Mellor and Yamada (1977) proposed an equation which is a variant of Rotta's (1951) equation, i.e.,

$$\frac{\partial (b^2 \ell)}{\partial t} = \frac{\partial}{\partial z}\left(b \ell \; S_\ell \frac{\partial}{\partial z}(b^2 \ell) \right)$$

$$- \ell \, E_1 \left[-\overline{uw}\frac{\partial u}{\partial z} - \overline{vw}\frac{\partial v}{\partial z} + \frac{g}{\theta_0}\overline{w\theta_v} \right]$$

$$- \frac{b^3}{B_1}\left\{ 1 + E_2 \left(\frac{\ell}{k_0 z} \right)^2 \right\} \qquad (3.24)$$

S_ℓ is a stability function related to λ_1 in the equation of b^2, and E_1 and E_2 are empirical constants. Z is the distance from the earth's surface. Mellor and Yamada (1977) uses: $(E_1, E_2, S_\ell)=(1.8, 1.33, 0.2)$.

Within the whole framework of the turbulence closure model, the determination of this turbulent length scale is a weakest area. However, it is true that the final results are rather insensitive to the choice of ℓ. Readers refer to Mellor and Yamada (1982).

Yokoyama et al. (1979) collected various observational values of the turbulence scale (Table 1). Figure 3.1 shows these values (dashed lines and solid lines). At $Z=10^3$m, the length scale ℓ falls in 100 ~ 400 m. Yokoyama et al. compared these data with the values of a formula

Fig. 3.1

$$\ell = kZ\left(1+\beta\frac{Z}{h}\right)^{-1}, \qquad (3.25)$$

where h is the depth of PBL. The formula's values of $\beta=0$, 2 and 4 are plotted by the solid lines. It appears, $\beta=2 \sim 4$ fit the observations.

Figures 3.2 ~ 3.5 are the results of a GCM based on E-physics. All variables are for 00GMT, 15 March, 1965, which is the 10th day in the predictions.

Fig. 3.2
3.3
3.4
3.5

Figure 3.2 is the latitude-height distribution of the zonally averaged turbulent kinetic energy. It is pronounced that two or three maxima are included in the vertical. One is the lowest layer, and the second is below the jet stream level in the middle latitudes and is at the tropopause level in the equatorial region. It would be worthy to note that turbulent energy

Table 1. Key to the scales of turbulence given in Fig. 1 and additional information.

No.	Authors	Additional information
3	Lettau (1950)	Neutral condition
4	Clarke (1970)	Clarke's class III (near neutral)
5	Yokoyama (1971)	$\|z/L\| \leq 1$ (near neutral)
6	Gamo and Yokoyama (1971)	Strong wind, by tethered balloon
7	Gamo et al.	Forced convection (KAW-MAR-1972)
8	Busch and Panofsky (1968)	Unstable
9	Kukharets and Tsvang (1969)	Summer, developed convection
10	Clarke (1970)	Clarke's class I (deep convection)
11	Clarke (1970)	Clarke's class II (shallow convection)
12	Yokoyama (1971)	$z/L < -1$ (unstable)
13	Warner (1972)	Convective situations (above the sea)
14	Gamo et al.	Free convection (KAW-MAR-1972)

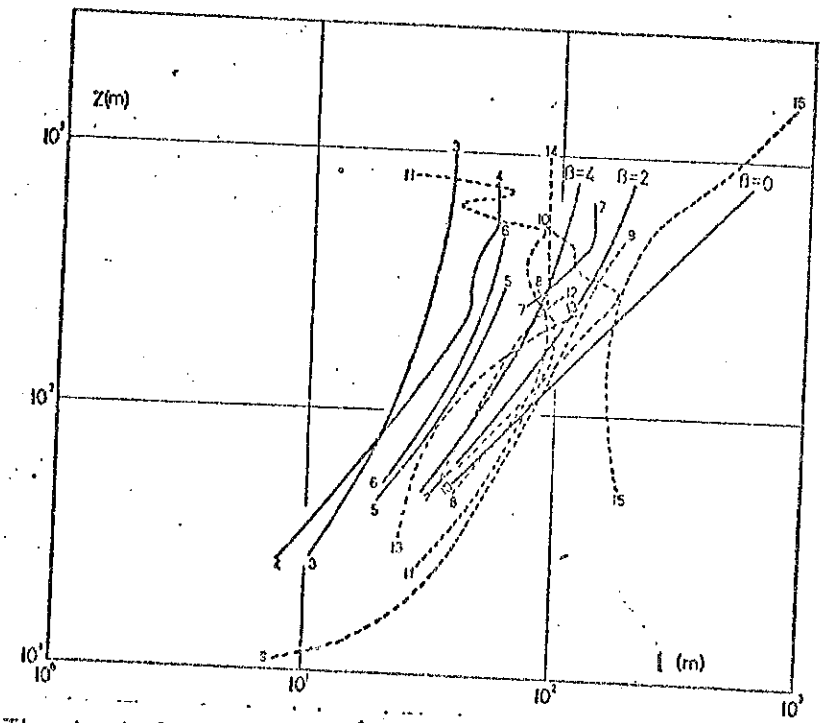

Fig. 3.1 The turbulence scale ℓ. Numbers indicate the papers cited in Table 1. Solid lines are for neutral condition, and dashed lines for unstable conditions, and the solid lines of β= 0, 2 and 4 are based on the formula (3.32) (after Yokoyama et al. 1979).

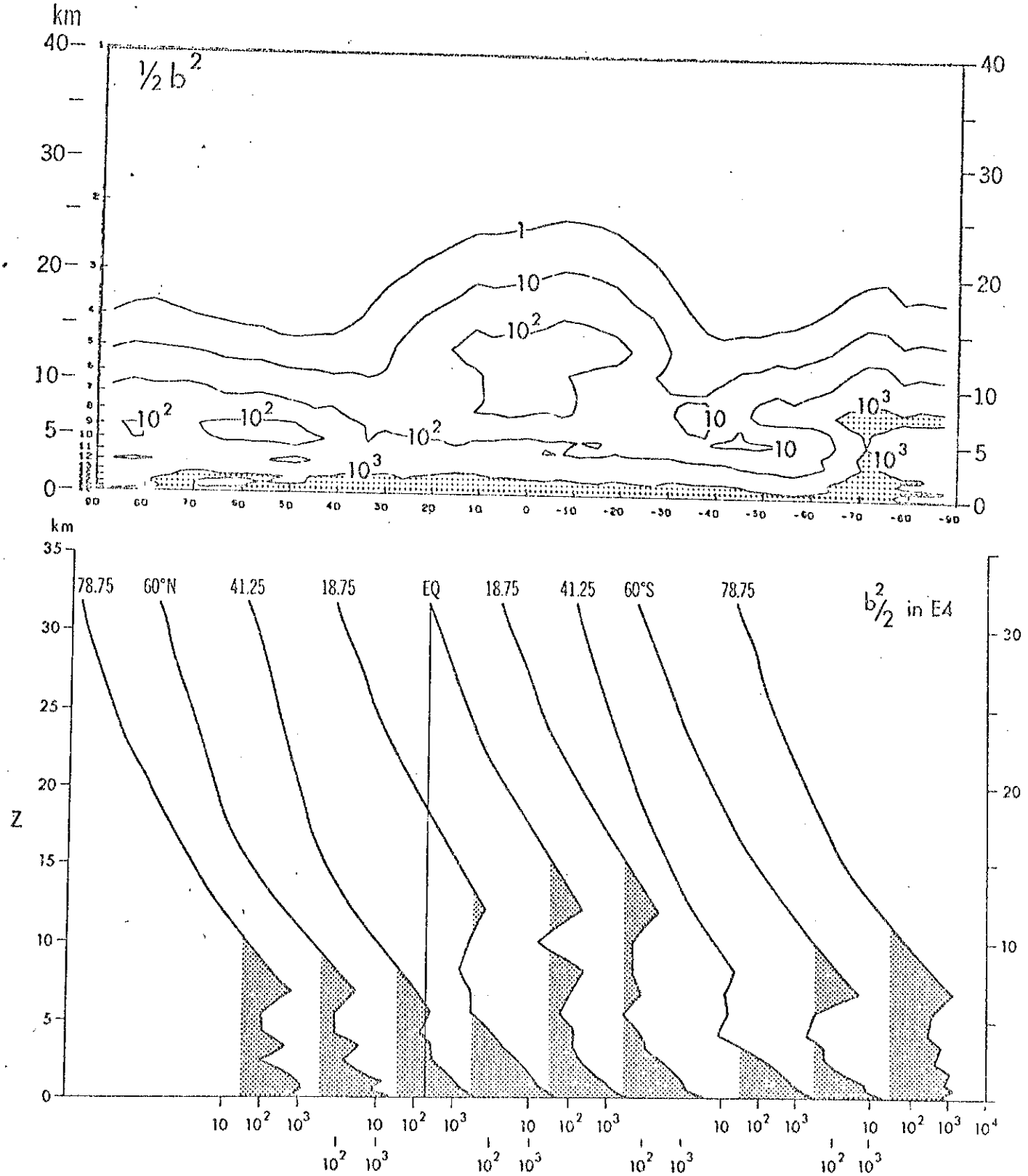

Fig. 3.2 Turbulent kinetic energy, 1/2 b^2, in the latitude-height section (upper) and the vertical distributions of 1/2 b^2 at selected latitudes (lower) in units of cm^2s^{-2}. In the upper panel, the region in which 1/2 $b^2 > 10^3$ is shaded, and in the lower panel, the layers in which 1/2 $b^2 > 2 \times 10^2$ are shaded.

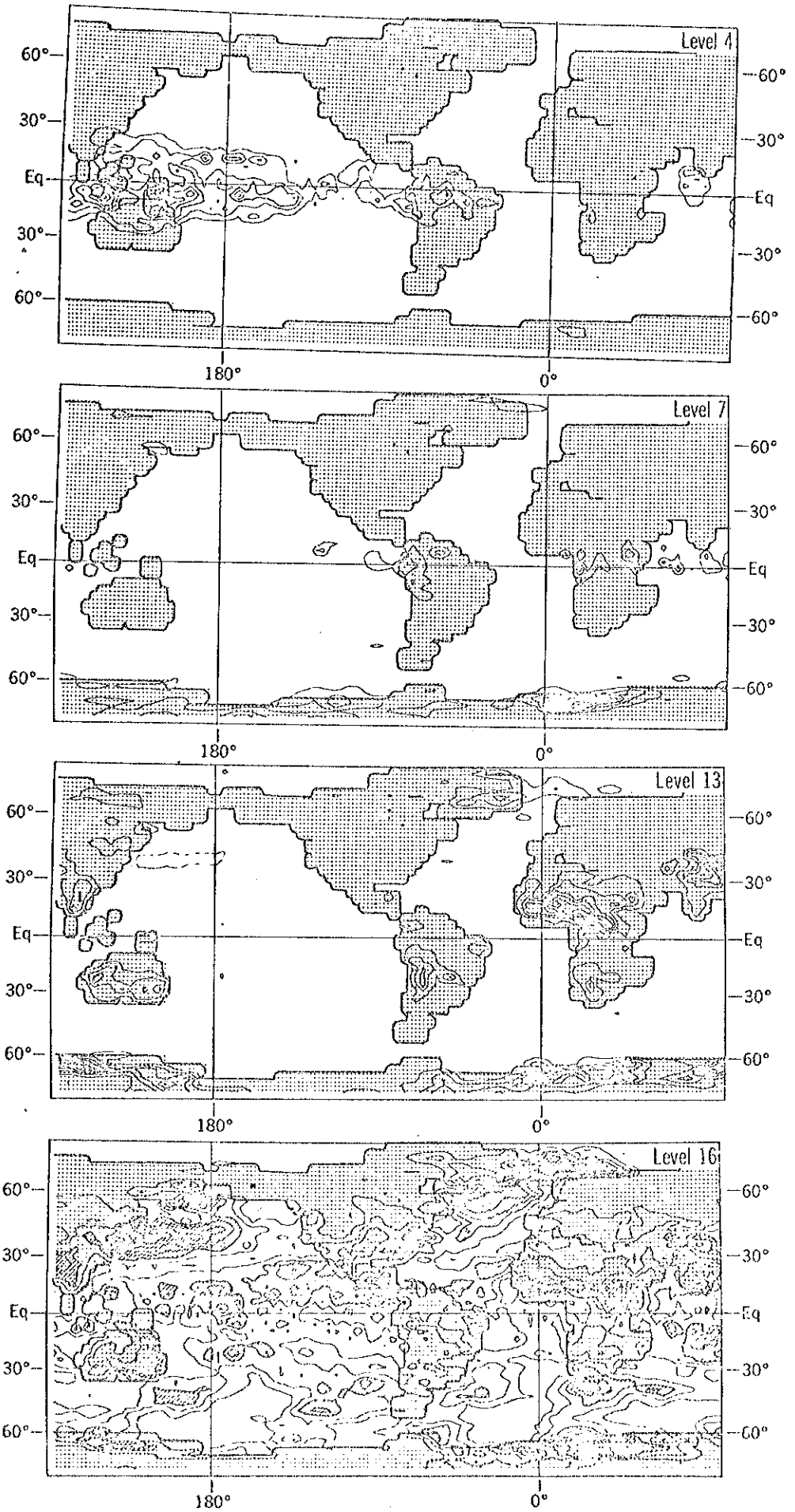

Fig. 3.3 Horizontal distribution of 1/2 b^2 at model's level 4 (99 mb), level 7 (297 mb), level 13 (777 mb) and level 16 (948 mb).

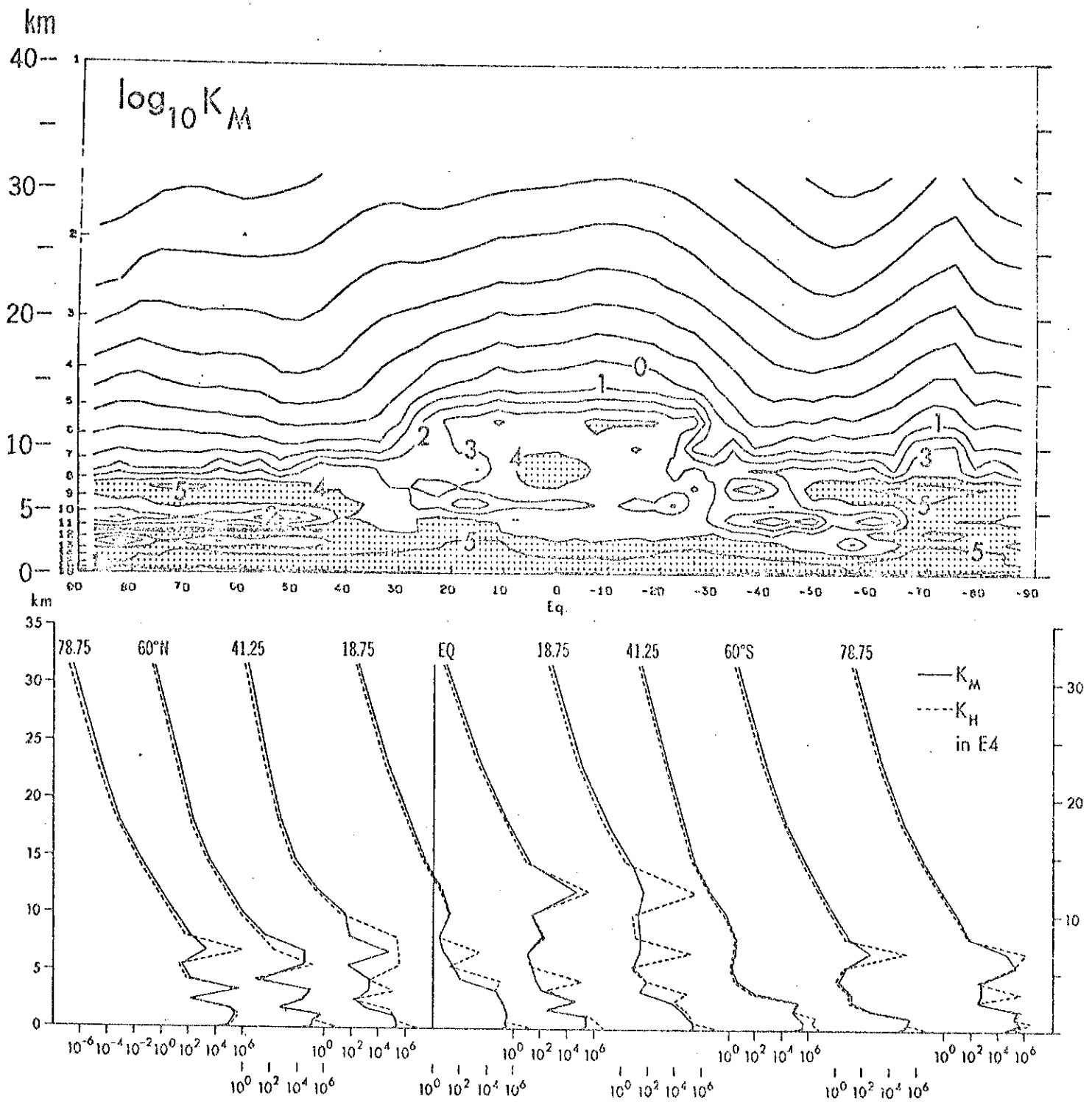

Fig. 3.4 The eddy viscosity $\log_{10}(K_M)$ and $\log_{10}(K_H)$ based on (3.12) and (3.13), respectively, which are revealed in the run of E-physics model. The upper panel is the latitude-height distribution of $\log_{10}(K_M)$. The contour interval is 10 in $\log_{10}(K_H)$, where K_M is in units of c.g.s. The area in which K_M is larger than 10^4 are shaded. The lower panel is the vertical profiles of $\log_{10}(K_M)$ and $\log_{10}(K_H)$ at selected latitudes (after Miyakoda and Sirutis, 1977).

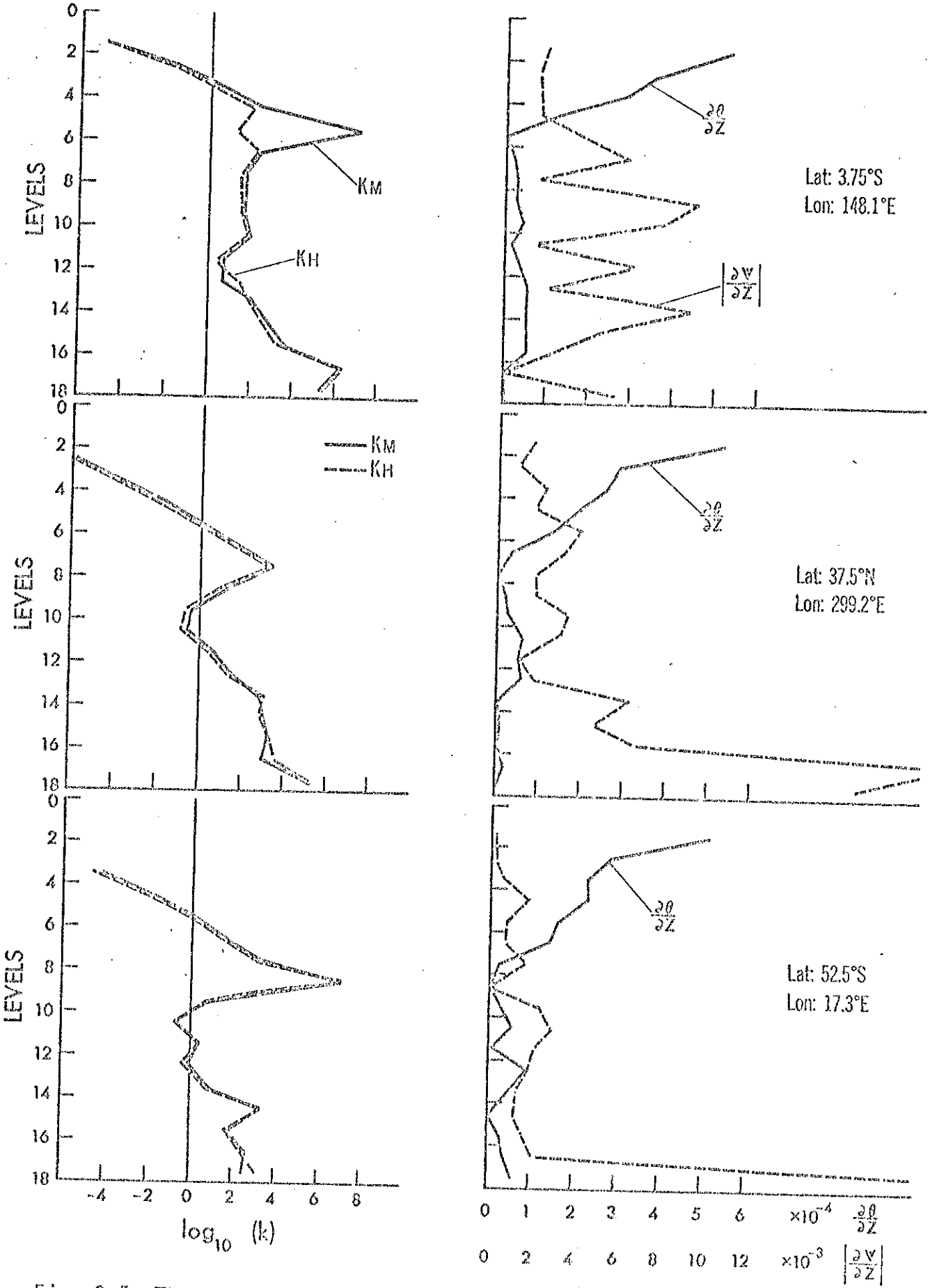

Fig. 3.5 The vertical distributions of K_M and K_H (left) and of $\frac{\partial \theta}{\partial z}$ and $\left|\frac{\partial V}{\partial z}\right|$ (right) at three geographical locations in units of c.g.s.

is found even above PBL. Figure 3.3. is the horizontal distribution at various levels. Level 16 corresponds to the upper portion of PBL. Turbulent energies are larger over continents, western boundary of the oceans, i.e., over Kuroshio or Gulf Stream, ITCZ and the regions of stratocumulus-topped PBL. Turbulence at level 13 is dominantly large over continents, particularly the Sahara desert, Himalaya, and continents of the Southern Hemisphere (summer). At level 4, turbulence is large over the cumulous convection area. The Indonesian Archipelago and Amazon basin are outstanding.

Figure 3.4 is the eddy viscosities, K_M and K_H, which are based on eqs. (3.12) and (3.13). It is interesting to note that K_H is larger than K_M in the troposphere (coinciding with eq. (2.11')). In order to see which factors contribute most to the large values of K_M and K_H, the comparative display is made with the thermal stratification in terms of $\partial\theta/\partial z$ and the vertical shear $|\partial\psi/\partial z|$ in figure 3.5. In general, when $\partial\theta/\partial z \to 0$, K_M and K_H become large except at the top panel. However, the association of turbulent kinetic energy with $\partial\theta/\partial z$ and $|\partial\psi/\partial z|$ is not simple, indicating that the effect of the level 2.5 model over that of level 2 model is appreciable.

3.5 Comment on the lateral viscosity

The formulation of non-linear lateral viscosity (2.12) is derived from the turbulence closure model of hierarchy level 1 or even simpler (Lilly, 1967; Deardorff, 1971, 1973a,b).

$$\frac{\partial q^2}{\partial t} \quad (\text{from} \quad (3.4')\ );$$

$$0 = -\frac{1}{2} A_{ij} D_{ij} + \frac{g}{\theta_0} w\theta - \frac{C_\varepsilon}{2^{3/2}} \frac{q^3}{\Delta} \qquad (3.26)$$

$\frac{\partial A_{ij}}{\partial t}$ (from (3.7')):

$$0 = -\frac{2}{15} b^2 D_{ij} - \frac{C_m}{2^{1/2}} \frac{b}{\Delta} A_{ij} \qquad (3.27)$$

$\frac{\partial \overline{u_i \theta}}{\partial t}$ (from (3.8')):

$$0 = -\frac{1}{3} b^2 \frac{\partial \theta}{\partial x_i} - C_s \frac{b}{2^{1/2}\Delta} \overline{u_i \theta} + \frac{2}{3} \delta_{i3} \frac{g}{\theta_0} \theta^2 \qquad (3.28)$$

The problem of the lateral viscosity is not related to the buoyancy, so the term with slash is not used. Combination of the terms of mechanical conversion and dissipation in (3.26), and (3.27) leads to

$$b^2 = \frac{4}{15} \frac{\Delta^2}{C_E \cdot C_m} D^2 \qquad (3.29)$$

Next insertion of (3.29) into (3.27) gives

$$A_{ij} = -\left\{ \frac{\frac{4}{15}\left(\frac{2}{15}\right)^{1/2}}{C_E^{1/2} C_m^{3/2}} \Delta^2 \cdot D \right\} D_{ij} \qquad (3.30)$$

Likewise, insertion of (3.29) into (3.28) gives

$$\overline{u_i \theta} = -\left\{ \frac{\frac{2}{3}\left(\frac{2}{15}\right)^{1/2}}{C_s \cdot C_E^{1/2} C_m^{1/2}} \cdot \Delta^2 \cdot D \right\} \frac{\partial \theta}{\partial x_i} \qquad (3.31)$$

C in (2.12) is, therefore, written by

$$C = \left(\frac{4}{15}\right)^{3/4}\left(C_E \cdot C_m^{\,3}\right)^{-1/4} \tag{3.32}$$

and $C_S = C_m$.

Thus

$$A_{ij} = -\left\{\frac{(C\cdot\Delta)^2}{\sqrt{2}} D\right\} D \tag{3.33}$$

$$\overline{u_i\theta} = -\frac{5}{2}\left\{\frac{(C\cdot\Delta)^2}{\sqrt{2}} D\right\}\frac{\partial\theta}{\partial x_i} \tag{3.34}$$

Assuming, as in (3.15), that C_m=4.13, C_E=0.70, C_θ=0.58, C is given by

$$C = 0.14\,, \tag{3.35}$$

where 5/2 in (3.34) was derived by Schemm and Lipps (1976), though this point is controversial.

4. Surface Layer

Near the earth's surface, the molecular viscosity plays a major role in vertical transfer of heat, moisture and momentum. The turbulence develops only above a certain level, which is defined as the roughness height, Z_o. Once the turbulence starts, it is efficient in transferring heat, etc.

Yet, because of the proximity of heat source, the temperature difference can remain quite large. (For example, over sand desert, 25° ~ 50°C temperature difference is often found within 1 ~ 2 meters), and the thermal instability can continue to exist in a shallow layer (Figure 4.1).

The overall situation in this layer is that the vertical turbulent transfer is very strong and that there is no other balancing effect. For this reason, the vertical fluxes can be approximated to be constant with height.

This layer is technically called as "the constant-flux layer," which normally extends from the level of Z_o to about 20 meter height. Because of the assumption of constant-flux, simple formulas for eddy transfers can be obtained.

4.1 Monin-Obukhov theory

As mentioned earlier, because of computational economy, the model's layer between the surface and the lowest level is treated jointly as the surface layer, in which the molecular as well as the turbulent fluxes are combined, and the bulk transfer scheme based on the similarity theory is used instead of the turbulent closure scheme. The shortcoming of this arrangement is that only the vertical transfer is considered and other effects such as lateral advection, baroclinicity and the effect of pressure gradient in space are all ignored.

First let us re-denote

$$\tau_{xz} \longrightarrow \tau_x$$

$$\tau_{yz} \longrightarrow \tau_y$$

$$\tau_{\theta z} \longrightarrow -H/c_p$$

$$\tau_{qz} \longrightarrow -E$$

Thus the equations (2.1) - (2.4) are written

$$\frac{du}{dt} + \cdots\cdots = \frac{1}{\rho}\frac{\partial \tau_x}{\partial z} \qquad (4.1)$$

$$\frac{dv}{dt} + \cdots\cdots = \frac{1}{\rho}\frac{\partial \tau_y}{\partial z} \qquad (4.2)$$

$$\frac{d\theta}{dt} + \cdots\cdots = -\frac{1}{\rho}\frac{\partial H/c_p}{\partial z} \qquad (4.3)$$

$$\frac{dq}{dt} + \cdots\cdots = -\frac{1}{\rho}\frac{\partial E}{\partial z} \qquad (4.4)$$

where H, and E>0 if transfers are directed upward, and τ_x and τ_y>0 if downward. τ_x, τ_y, H and E at the surface layer are denoted by the suffix zero, i.e., τ_{ox}, τ_{oy}, H_o and E_o.

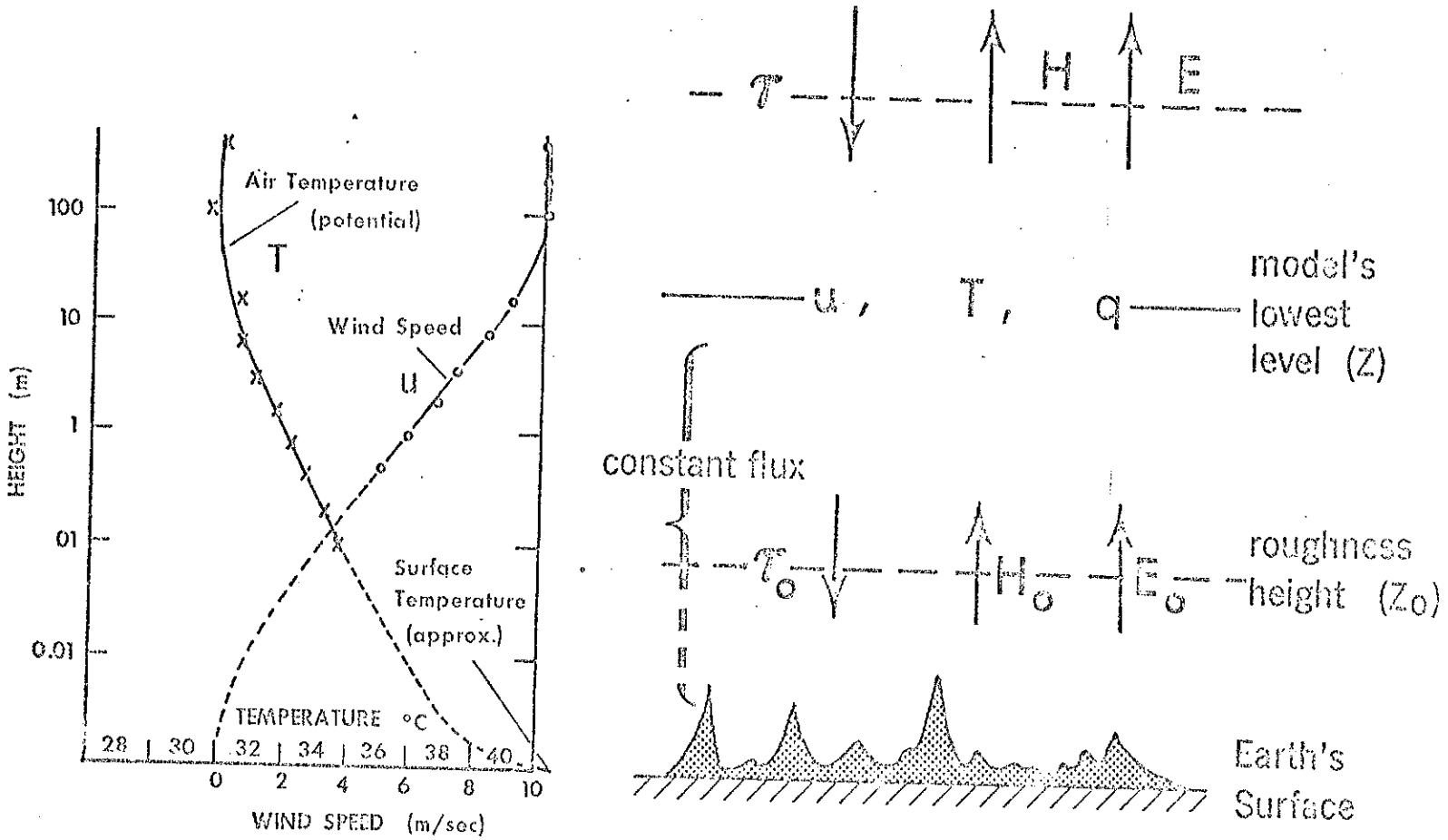

Fig. 4.1 The constant-flux layer. The vertical distributions of wind speed and potential temperature (left) (after Deacon), and the model's levels, wind stress, sensible and latent heat fluxes (right).

On the dimensional base, one can define a parameter, V_*, i.e., the friction velocity, which is constant in Z.

$$\tau_o/\rho = V_*^2 \qquad (4.5)$$

Where

$$\tau_o = \left(\tau_{ox}^2 + \tau_{oy}^2 \right)^{1/2} \tag{4.6}$$

$$V_* = \left(u_*^2 + v_*^2 \right)^{1/2} \tag{4.7}$$

Using this friction velocity, other fluxes are expressed as

$$\begin{aligned} \tau_{ox} &= \rho \cdot |V_*| \cdot u_* \\ \tau_{oy} &= \rho \cdot |V_*| \cdot v_* \end{aligned} \tag{4.8}$$

$$H_o / c_p = - \rho \cdot |V_*| \cdot \theta_* \tag{4.9}$$

$$E_o = - \rho \cdot |V_*| \cdot q_* \tag{4.10}$$

where u_*, v_*, θ_* and q_* are the new parameters with the respective dimension.

Monin and Obukhov (1954) developed theories on the vertical gradients of wind, temperature and moisture as

$$\frac{k_o z}{u_*} \frac{\partial u}{\partial z} = \varphi_m(z)$$

$$\frac{k_o z}{v_*} \frac{\partial v}{\partial z} = \varphi_m(z) \tag{4.12}$$

$$\frac{k_o z}{\theta_*} \frac{\partial \theta}{\partial z} = \varphi_h(z) \tag{4.13}$$

$$\frac{k_0 z}{q_*}\frac{\partial q}{\partial z} = \varphi_q(z) \tag{4.14}$$

where k_0 is Karman constant ($\equiv 0.41$), ϕ_m, ϕ_h and ϕ_q are the Monin-Obukhov similarity function, which are known to be unity in the neutral case. They introduced a length scale (Monin-Obukhov length) L_{mo}, which consists of heat flux $H_0/\rho c_p$ (and exactly speaking, the heat flux based on the virtual temperature ($H_0/c_p + 0.61 \cdot T_{00} \cdot E_0$), the acceleration of gravity, g, the reference temperature, T_{00}, and the friction velocity, V_*.

$$L_{mo} = \frac{-T_{00} \cdot V_*^3}{k_0 g \left(H_0/\rho c_p + 0.61 \cdot T_{00} \cdot E_0/\rho \right)} \tag{4.15}$$

where $L_{mo} > 0$ if the stratification is stable and $L_{mo} \leq 0$ if it is unstable. A dimensionless quantity is

$$\zeta = z/L_{mo} \tag{4.16}$$

which is shown to be related to the stability index or the thermal stratification (Richardson number).

Using ζ, eq. (4.12) - (4.14) are first non-dimensionalized and then integrated with respect to ζ as

$$f_m(\zeta) = \frac{1}{k_0}\int \frac{\varphi_m(\zeta)}{\zeta} d\zeta \tag{4.17}$$

Thus

$$u(z) - u(z_0) = u_* \left[f_m(\zeta) - f_m(\zeta_0) \right] \quad (4.18)$$

$$v(z) - v(z_0) = v_* \left[f_m(\zeta) - f_m(\zeta_0) \right] \quad (4.18')$$

$$\theta(z) - \theta(z_0) = \theta_* \left[f_h(\zeta) - f_h(\zeta_0) \right] \quad (4.19)$$

$$q(z) - q(z_0) = q_* \left[f_h(\zeta) - f_h(\zeta_0) \right] \quad (4.20)$$

where $\zeta_0 = Z_0/L_{mo}$, $f_h(\zeta) = f_q(\zeta)$, and $u(Z_0) = v(Z_0) = 0$.

Let us denote

$$F_M = f_m(\zeta) - f_m(\zeta_0) \quad , \quad (4.21)$$

$$F_H = f_h(\zeta) - f_h(\zeta_0) \quad , \quad (4.22)$$

Using (4.21) - (4.22), the eq. (4.18) - (4.20) are re-written as

$$u_* = \frac{u(z)}{F_M} \quad (4.23)$$

$$v_* = \frac{v(z)}{F_M} \quad (4.23')$$

$$\theta_* = \frac{\theta(z) - \theta(z_0)}{F_H} \quad (4.24)$$

$$q_* = \frac{q(z) - q(z_0)}{F_H} \quad (4.25)$$

The friction velocity (4.7) becomes

$$|V_*| = \frac{\left[u(z)^2 + v(z)^2\right]^{1/2}}{F_M}$$

$$= \frac{|V(z)|}{F_M} \qquad (4.26)$$

Therefore, insertion of (4.21) - (4.25) in (4.8) - (4.11) leads to

$$H_0/c_p = -\rho \cdot C_H \cdot [\theta(z) - \theta(z_0)] \qquad (4.27)$$

$$E_0 = -\rho \cdot C_H \cdot [q(z) - q(z_0)] \qquad (4.28)$$

$$\tau_{ox} = \rho \cdot C_D \cdot u(z) \qquad (4.30)$$

$$\tau_{oy} = \rho \cdot C_D \cdot v(z) \qquad (4.30')$$

$$C_D = \frac{|V(z)|}{F_M^2} \qquad (4.31)$$

$$C_H = \frac{|V(z)|}{F_M \cdot F_H} \qquad (4.31')$$

The stability, $Z/L_{mo} = \zeta$ in (4.16), is written as

$$\zeta = z/L_{mo}$$

$$= k_0 z \cdot g \frac{F_M^2}{F_H} \frac{\left[\theta(z) - \theta(z_0) + 0.61 \cdot T_{00}\left[q(z) - q(z_0)\right]\right]}{T_{00} \cdot \left[V(z)\right]^2} \quad (4.32)$$

4.2 Form of similarity functions

The stability dependence form of the Monin-Obukhov similarity function is determined empirically. There are numerous studies such as Dyer and Webb (1967), Paulson (1970), Dyer and Hicks (1970), Webb (1970), Clarke (1970a), Miyake and McBean (1970), Businger et al. (1971, Plate (1971), Monin and Yaglom (1966), Dyer (1974), Hicks (1976), Carson and Richards (1978), etc. The particular form employed in this manual is the one proposed by Businger et al. (1971) and Hicks (1976), i.e.,

$$\varphi_m = \begin{cases} (1 - 15 \cdot \zeta)^{-1/4} & \zeta < 0 \\ (1 + 5 \cdot \zeta) & 0 \le \zeta < 0.5 \\ \left(8 - \frac{4.25}{\zeta} + \frac{1}{\zeta^2}\right) & 0.5 \le \zeta < 6 \\ 0.76\,\zeta & 6 \le \zeta \end{cases} \quad (4.33)$$

$$\varphi_h = \begin{cases} (1 - 16\zeta)^{-1/2} & \zeta < 0 \\ \varphi_m & 0 < \zeta \end{cases} \quad (4.34)$$

See the comments of Carson and Richards (1978) about the case $6 \le \zeta$, Dyer (1974) about k_0. The similar formulas are used by Yamagishi (1980) in his prediction model.

Figures 4.2 and 4.3 show the overall feature of the function against ζ. In the unstable region ($\zeta<0.21$), there is no problem, whereas in the stable region of the profile of the curve posed a controversy. So far as we know (Carson and Richards, 1978), the Hick's formula is satisfactory.

Fig. 4.

Fig. 4.

Concerning the matching between the Monin-Obukhov theory in the surface layer and the turbulence closure model in the rest of PBL, Mellor (1973) derived the functional form of ϕ_m and ϕ_h as

$$\varphi_m \propto (1 - R_f)^{-1/4}$$

$$\varphi_h \propto (1 - R_f)^{-1/4}$$

for the constant-flux condition in the case of $R_f<0$, where R_f is the flux Richardson number, and is related to ζ as $\zeta = \phi_m R_f$. This implies that turbulence closure scheme is almost consistent to the Hick's empirical formulas, (4.33) and (4.34), so far as the unstable case is concerned.

Integration of the equations

$$f_m(\zeta) = \frac{1}{k_0} \int \frac{\varphi_m(\zeta)}{\zeta} d\zeta \qquad (4.35)$$

$$f_h(\zeta) = \frac{1}{k_0} \int \frac{\varphi_h(\zeta)}{\zeta} d\zeta \qquad (4.36)$$

can be performed analytically for the formulas of ϕ_m, (4.33), and $\phi_h(\zeta)$, (4.34). (Paulson, 1970; Nickerson and Smiley, 1975; Benoit, 1977).

For $\zeta<0$

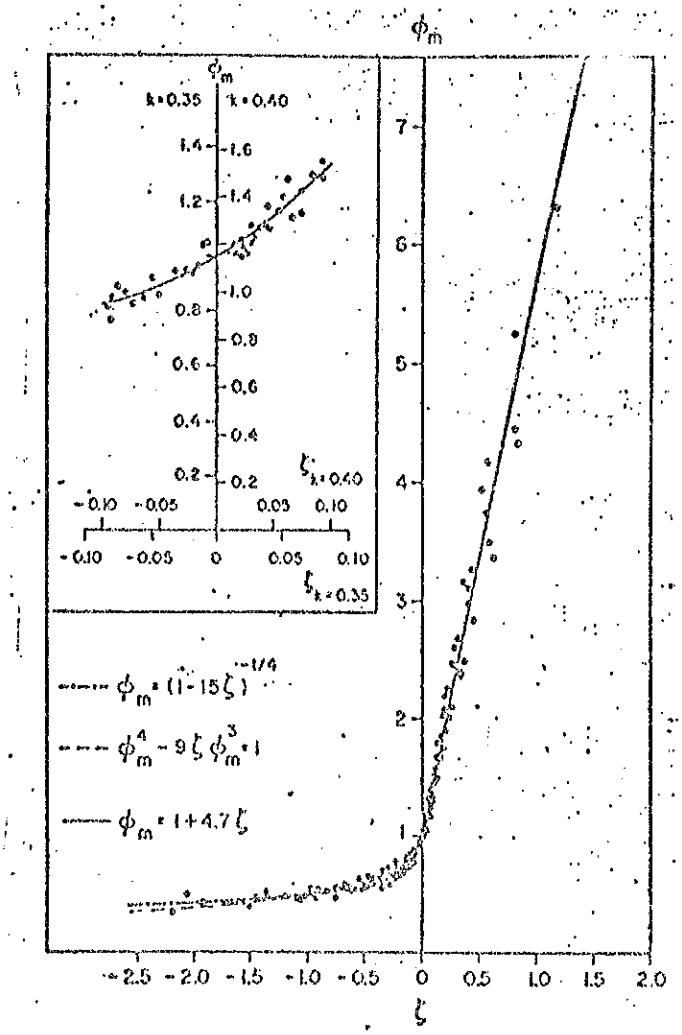

Fig. 4.2 Similarity functions ϕ_m and observations (after Businger et al. 1971.)

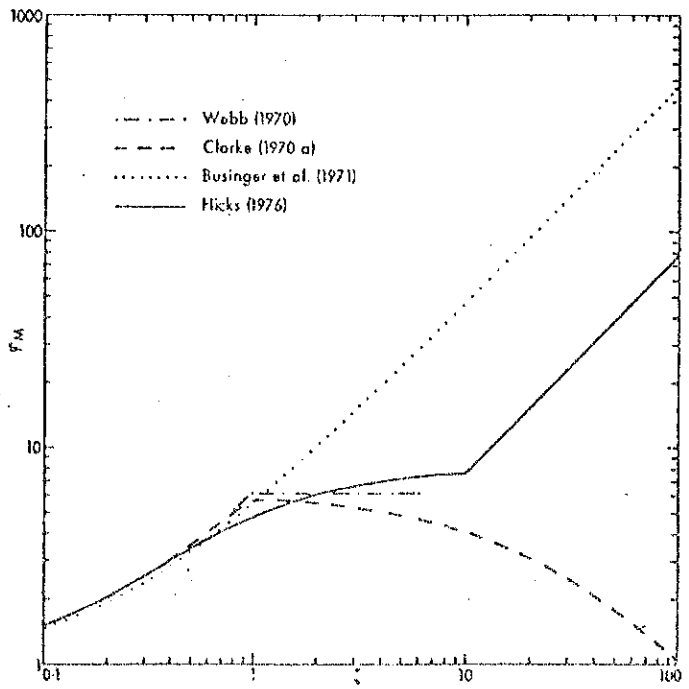

Fig. 4.3 Various similarity functions ϕ_m in the stable condition (after Carson and Richards, 1978).

$$f_m(\zeta) = \frac{1}{k_0}\left[2\cdot\tan^{-1}x + \ln\left(\frac{1-x}{1+x}\right)\right] \quad (4.37)$$

where $X = (1 - 15\cdot\zeta)^{1/4}$

$$f_h(\zeta) = \frac{1}{k_0}\ln\left|\frac{Y-1}{Y+1}\right| \quad (4.38)$$

where $Y = (1-16\zeta)^{1/2}$.

for $0 \leq \zeta \leq 0.5$

$$f_m(\zeta) = f_h(\zeta) = \frac{1}{k_0}(\ln\zeta + 5.5) \quad (4.39)$$

for $0.5 \leq \zeta \leq 10.0$

$f_m(\zeta) =$

$$f_h(\zeta) = \frac{1}{k_0}\left(8\ln\zeta + \frac{4.25}{\zeta} - \frac{1}{2\zeta^2} + 0.852\right) \quad (4.40)$$

for $10.0 \leq \zeta$

$$f_m(\zeta) = f_h(\zeta) = (0.76\zeta + 7.093) \quad (4.41)$$

The constants 0.852 in (4.40) and 7.093 in (4.41) are determined so that $f_m(\zeta)$ be continuous at $\zeta = 0.5$ and 10.0.

Therefore, F_M and F_H are given according to (4.21) and (4.22) as

$\zeta < 0$

$$F_M = \frac{1}{k_0}\left\{ \ln \frac{z}{z_0} - \ln \left[\frac{(1+X_0)^2(1+X_0^2)}{(1+X)^2(1+X^2)}\right] + 2\left(\tan^{-1}X - \tan^{-1}X_0\right)\right\} \quad (4.42)$$

where $x = (1 - 15\zeta)^{1/4}$

$$F_H = \frac{1}{k_0}\left\{ \ln \frac{z}{z_0} - 2 \ln \left(\frac{Y+1}{Y_0+1}\right)\right\} \quad (4.43)$$

where $Y = (1-16\zeta)^{1/2}$

$0 \leq \zeta \leq 0.5$

$$F_M = F_H = \frac{1}{k_0}\left[\ln \frac{z}{z_0} + 5(\zeta - \zeta_0)\right] \quad (4.44)$$

$0.5 \leq \zeta \leq 10$

$$F_M = F_H = \frac{1}{k_0}\left[8 \cdot \ln \frac{z}{z_0} + 4.25\left(\frac{1}{\zeta} - \frac{1}{\zeta_0}\right) - \frac{1}{2}\left(\frac{1}{\zeta^2} - \frac{1}{\zeta_0^2}\right)\right] \quad (4.45)$$

$10 \leq \zeta$

$$F_M = F_H = \frac{1}{k_0} 0.76 (\zeta - \zeta_0) \quad (4.46)$$

(See Fig. 4.4 and Fig. 4.5.)

4.3 Land surface roughness

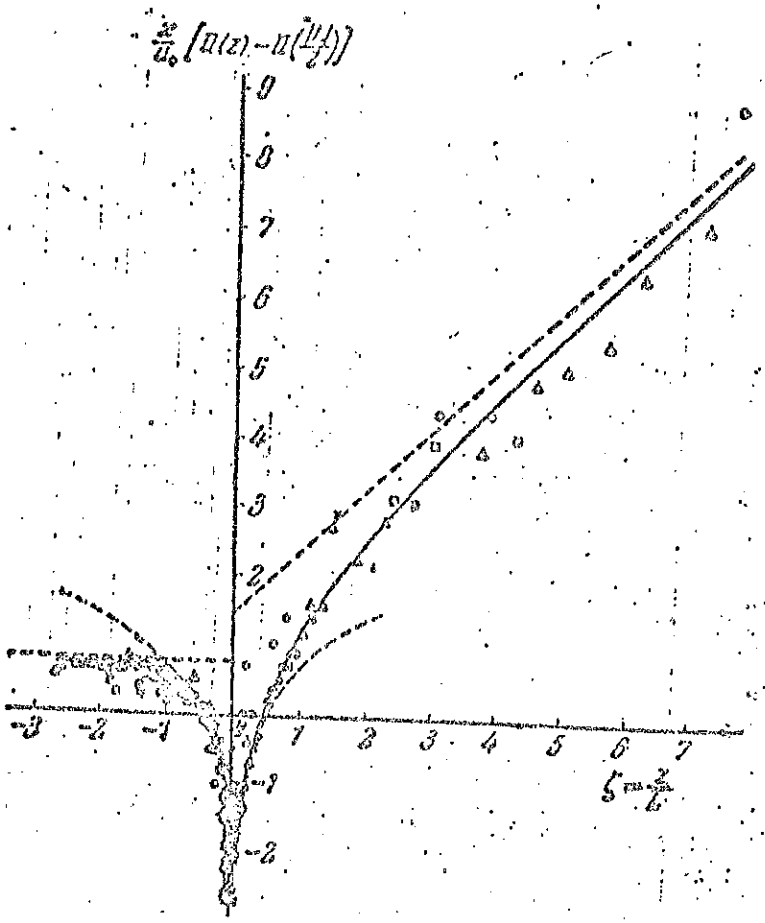

Fig. 4.4 Similarity function $f(\zeta)$ (after Monin and Obukhov, 1954).

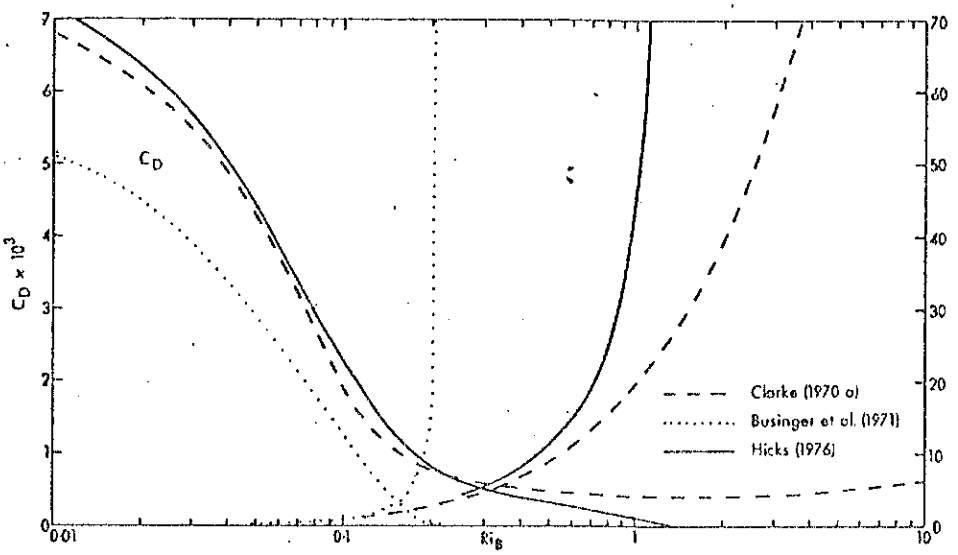

Fig. 4.5 The drag coefficient C_D for z = 10 m and z_0 = 0.1 m as functions of the bulk Richardson number, Ri_B. The curves have been derived from the indicated observational studies (after Carson and Richards, 1978).

The exchange coefficients, C_D and C_H in (4.31) are determined by the roughness length Z_0 and the height level Z and also by the thermal stratification z/L_{mo}. In the neutral case, C_D and C_H are reduced to

$$C_D = C_H = [\, k_o / \ln (z/z_0) \,]^2 \qquad (4.47)$$

The most pronounced fact is that the roughness length varies considerably if the mountain range is involved (see the review of Garratt, 1977).

a. Flat terrain

The local roughness Z_0 is determined by the physical and vegetational structure of the surface. Kung and Lettau (1961) and Kung (1963) determined the vegetation distribution from a number of sources, and estimated Z_0 over continental land masses. The table of Kung's C_D indicates that Z_0 becomes larger in summer than in winter, because of trees which have more leaves and grasses in summer.

Table 1.

Kung's C_D at anemometer level

winter	3.30×10^{-3}
summer	5.24×10^{-3}

See Footnote.

In the E-physics, however, the annual mean Z_0 is used, i.e.,

$$Z_0 = 16.82 \text{ cm} \qquad (4.48)$$

Figure 4.6 shows the normalized drag coefficient C_D, i.e., C_D/C_{DN} as a

Fig. 4.6

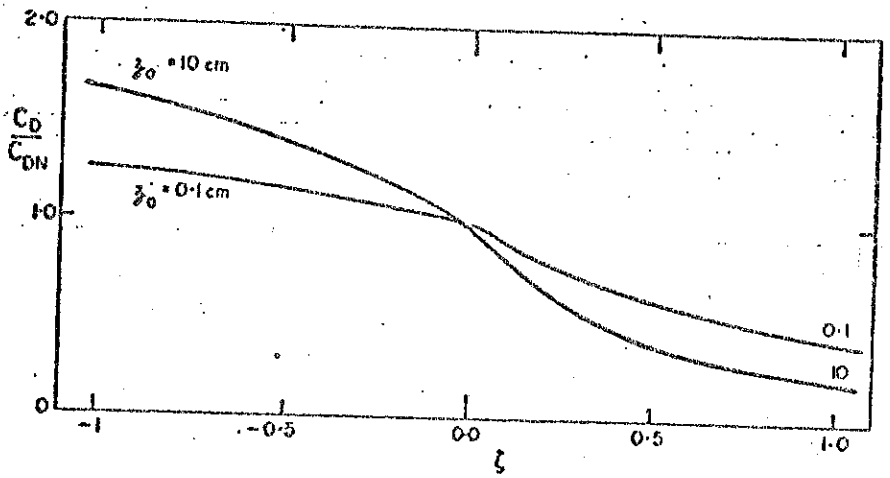

Fig. 4.6 Variation of C_D/C_{DN} (reference height of 10 m) for two values of Z_o on empirical stability functions of Dyer and Hicks (1970) and Webb (1970).

function of stability $\zeta = Z/L_{mo}$, where C_{DN} is the neutral drag coefficient.

b. Mountainous region

The influence of uneven topography increases considerably the aerodynamic roughness and hence, the total stress. The addition of form drag is accounted for by increasing C_D and Z_0.

Fiedler and Panofsky (1972) used turbulence observations made from an aircraft to show that Z_0 over mountainous areas was some 2 ~ 3 times larger than for the plains. Cressman (1960) used a simple formula to calculate form drag which was derived from Sawyer's (1959) treatment of gravity wave momentum transfer arising from flow perturbation over mountain ridges (Figure 4.7). This gave a C_D of 8.5×10^{-3} for the Rockies or Himalayas and 1.5×10^{-3} for the Appalachians, which is compared with 1.2×10^{-3} for the frictional (vegetation) drag of land surfaces.

Fig. 4.

The exact treatment of mountain form drag is very difficult, -- Bleck (1977) used a heuristically designed formula as

$$C_D = .001 + .004 \times \frac{Z_*}{Z_* + 1000} \qquad (4.49)$$

where Z_* is in units of meter. This formula yields a value of 0.001 at sea level, 0.002 at 333 m, 0.003 at 1 km, and 0.004 at 3 km.

In this manual, we follow Gordon's formula

$$C_D = C_{DO} + .003 \times \left[\frac{Z_*}{Z_* + 1000} + \frac{Z_r}{Z_r + 1000} \right] \qquad (4.50)$$

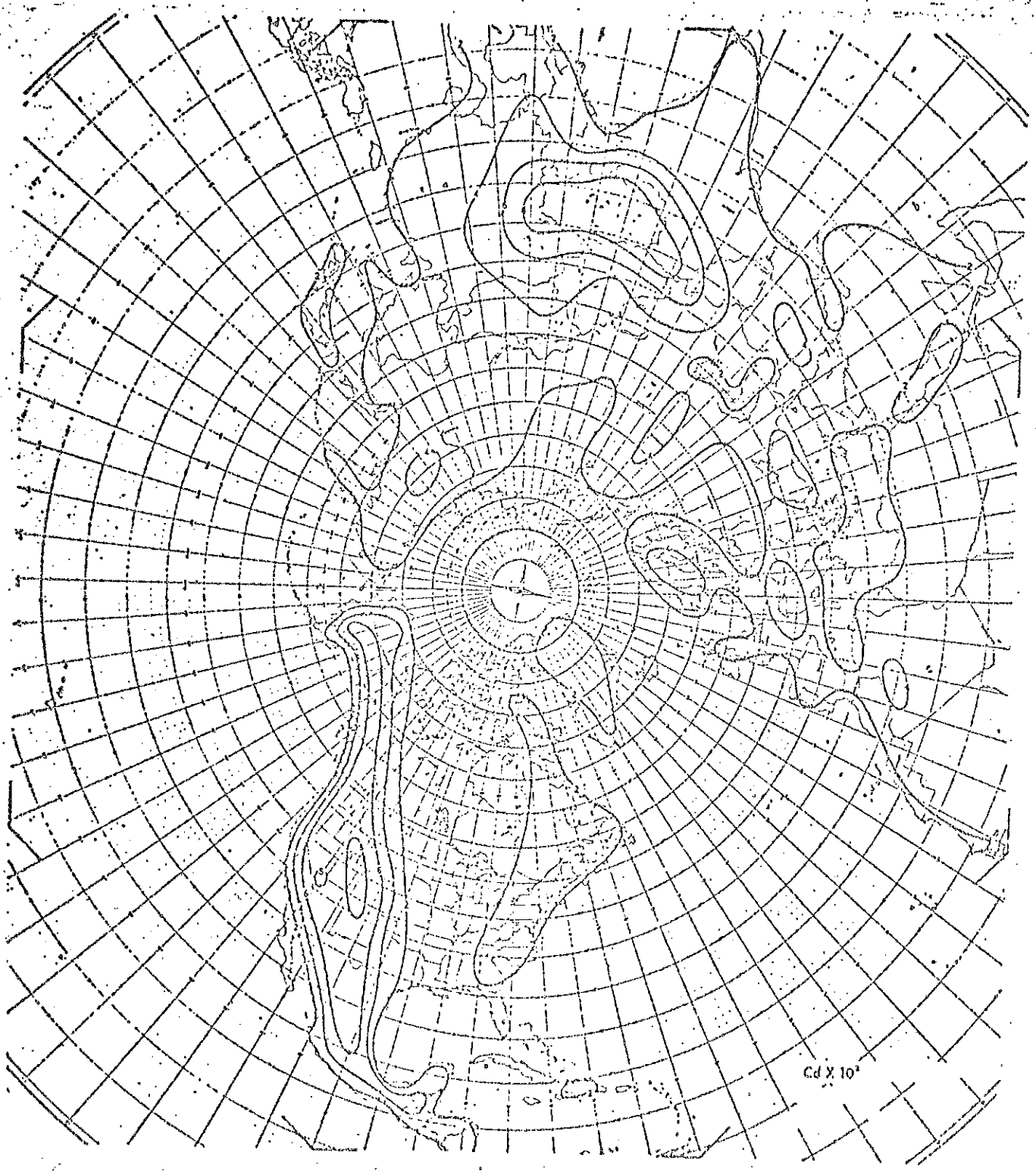

Fig. 4.7 Hemispheric map of mountain drag (after Cressman, 1960).

where Z_r is the spatial variance of topography within a grid box, and C_{DO} is the drag of non-mountainous component.

4.4 Ocean surface roughness

Charnock (1955) and Kitaigorodsky (1973) proposed the relation of the roughness length with the wind stress, based on the dimensional analysis,

$$z_o = \alpha \frac{u_*^2}{g} \qquad (4.51)$$

where g is the acceleration of gravity and α is non-dimensional constant. Note that this formula does not contain the coefficient of molecular viscosity.

Charnock relation, shown as a solid line in Fig. 4.8, is a good representation of the overall trend of the data for $U_{10}>5$ m s^{-1}. The line in the figure can be expressed as $z_0 = \alpha u_*^2/g$, $\alpha = 0.0185$. It has been shown (Wu, 1969) that Charnock constant depends on the value adopted for the von Kármán constant. The most recent review by Garratt (1977) provided $\alpha = 0.0144$ for $k_o = 0.41$.

Fig. 4.8

E-physics uses

$$z_0 = 0.032 \cdot \frac{V_*^2}{g} \qquad (4.52)$$

$$= 0.032 \cdot \left[V(z) / F_M \right]^2$$

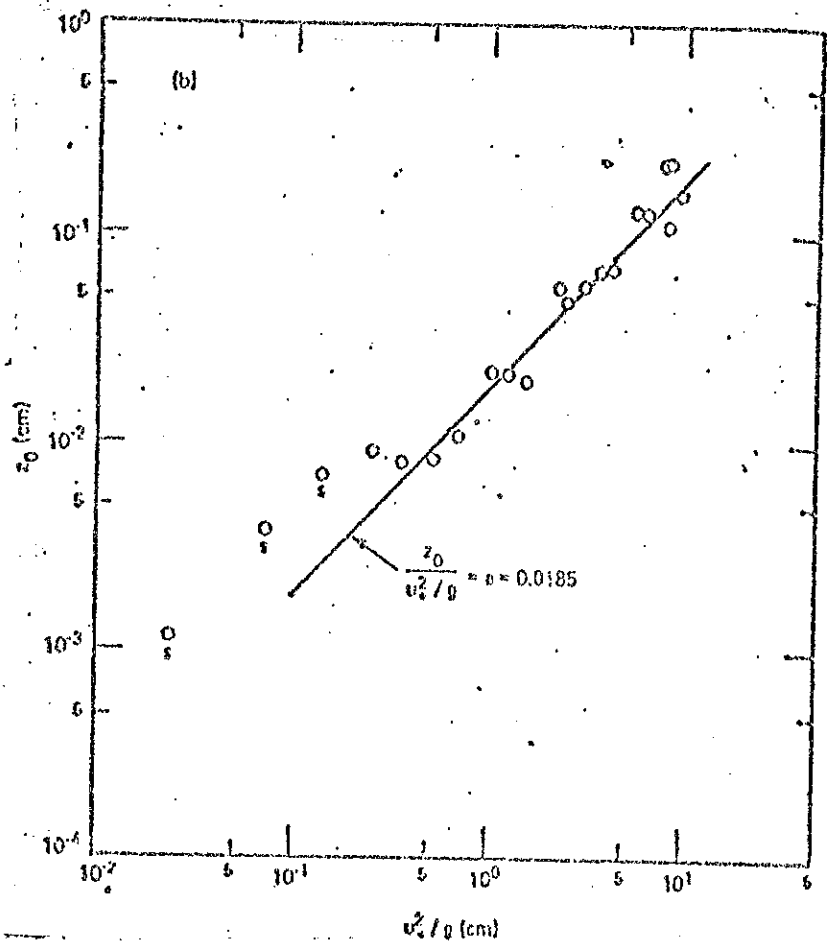

Fig. 4.8 Boundary-layer regimes and Charnock relationship (after Wu, 1972).

5. Surface Heat Balance

In the problem of long-term climate variability, a major interest is the ultimate balance of various types of energy at $t \to \infty$. On the other hand, in the problems of weather forecasts, the finite time response of the atmosphere to various causes is a serious and important issue.

A large portion of the incoming solar energy is absorbed by the earth's surface and is held at least for a short while. Figure 5.1 shows various components of energy that are relevant to the heat budget at the air-earth interface. R_n is the net radiation which is defined by

$$R_n = R_s^{\downarrow}(1-a) + R_L^{\downarrow} - \varepsilon \cdot \sigma \cdot T_s^4 \qquad (5.1)$$

where $R_S^{\downarrow}$ is the downward short-wave radiation, a is the albedo at the surface, $R_L^{\downarrow}$ is the downward long-wave radition, T_S is the surface temperature, $R_L^{\uparrow} = \varepsilon\sigma T_S^4$ is the upward long-wave radiation, and σ is the Stefan-Boltzman constant, and ε is the emissivity.

Fig. 5.1

At the ground surface, the net energy is written as

$$\text{net energy} = R_n - H_o - L \cdot E_o - L_f \cdot E_x \qquad (5.2)$$

where $L_f E_X$ is the heat used for melting snow or ice, and L_f is the latent heat of fusion. Over land, the soil heat conduction H_{soil} is included in the total balace, which is normaly equal to the influx to the ground, G, i.e., $H_{soil} = -G$.

Over land, the rate of evaporation E_o includes that of transpiration,

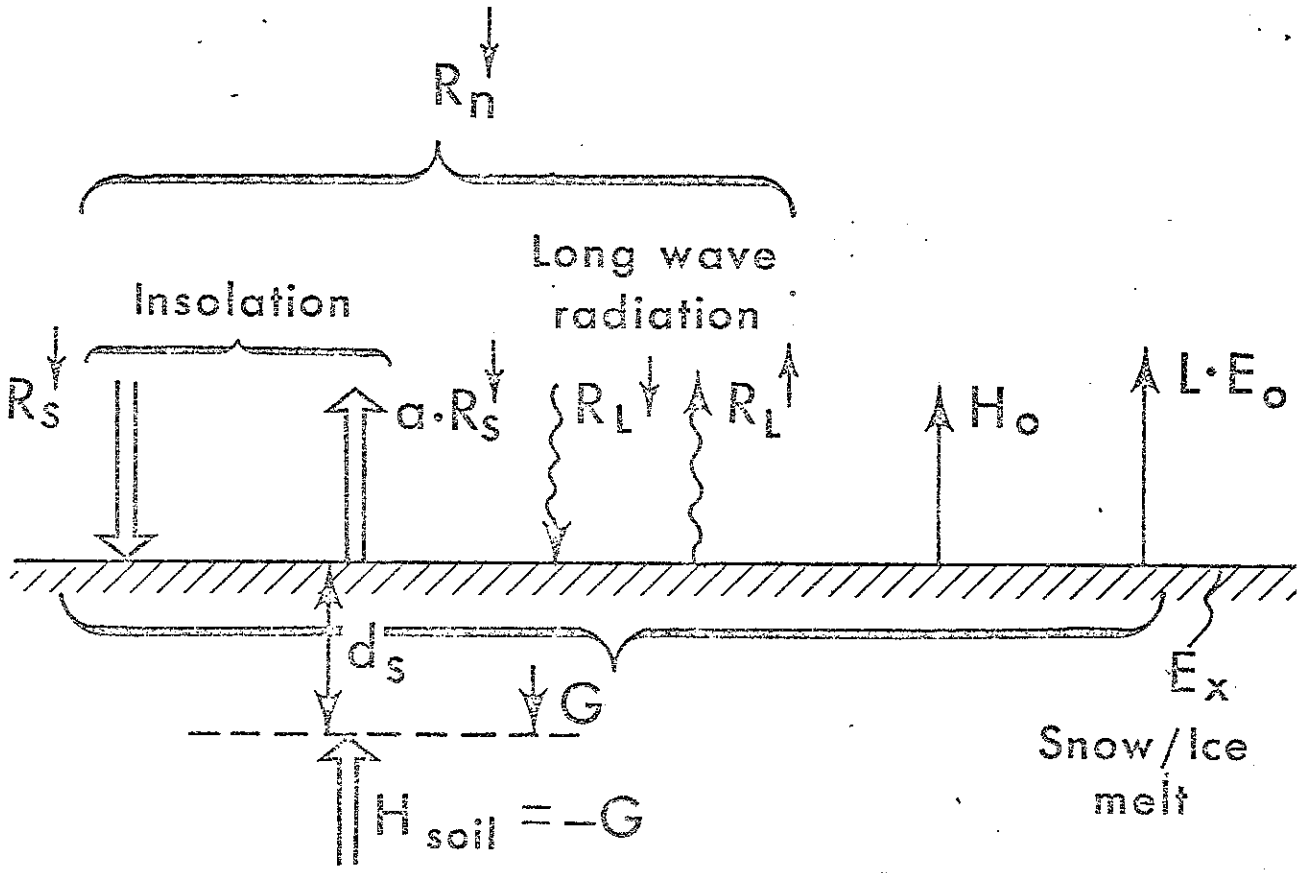
R_n
Insolation
Long wave radiation
R_s
$a \cdot R_s$
R_L
R_L
H_o
$L \cdot E_o$
d_s
G
E_x
Snow / Ice melt
$H_{soil} = -G$

which is associated with plants and grasses. This subject will be discussed in the next section. H_o and $L \cdot E_o$ are mutually related, and therefore, they are treated together. In this connection, hydrologists often refer to the Bowen ratio, i.e., $B_o = H_o / L \cdot E_o$.

5.1 Balance over land without snow/ice

The equation of surface heat budget is written as

$$R_n - H_o - L \cdot E_o - L_f \cdot E_x - G = 0. \qquad (5.3)$$

T_s is obtained by solving this equation, where $\varepsilon\sigma T_s^4$, H_o, E_o, and H_{soil} (or G) are functions of T_s. In order to solve this equation, Newton-Raphson's method is used, and the solution is reached iteratively.

This method is successful (Delsol et al. 1971) in producing reasonable results and has been used in the model until recently. However, it is very complicated and very inefficient computationally. For this reason it has been replaced by the prognostic method described below.

The time-dependent prognostic equation is set up (Arakawa, 1972; Corby et al. 1972) as

$$\frac{\partial C_s \cdot \rho_s \cdot d_s \cdot T_s}{\partial t} = R_n - H_o - L \cdot E_o - L_f \cdot E_x - G \qquad (5.4)$$

where C_s is the heat capacity of soil, ρ_s is the density, and d_s is the thickness of soil layer.

These factors, C_s, ρ_s and d_s together with the thermal conductivity in G determine the thermal inertia, and accordingly, the oscillation of the solution for T_s. The amplitude of diurnal variation of T_s and the diurnal

phase relation between T_S, R_S and G are controlled by these factors. The constant d_S and the thickness of next soil layer (see figure 5.3) are chosen to yield the exact solution for a sinusoidally varying soil surface heat flux G. In our case, d_S=5 cm (Bhumralkar, 1975, used 1 cm) (see Deardorff, 1978).

At any rate, the final prognostic results of surface temperature and pressure appears to be acceptable despite the artificiality mentioned above, and in fact, the prediction is better in terms of the 500 mb geopotential height skill score than in the previous version which used the balance solution.

From (4.27), H_0 is (figure 5.2)

Fig. 5.2

$$H_o/C_p = -\rho \cdot C_H [\theta(z) - \theta(z_o)] \quad (5.5)$$

Over land, E_0 depends critically on the availability of moisture, so instead of eq. (4.28), the relation

$$E_o = \beta \cdot E_{pot} \quad (5.6)$$

is used. Where E_{pot} is the rate of potential evaporation (Thornthwaite, 1948), and β is the availability of soil moisture, E_{pot} is tentatively written as

$$E_{pot} = -\rho \cdot C_H [q(z) - q_{sat}(T_s)] \quad (5.7)$$

where $q_{sat}(T_s)$ is the saturated moisture at the surface temperature T_s.

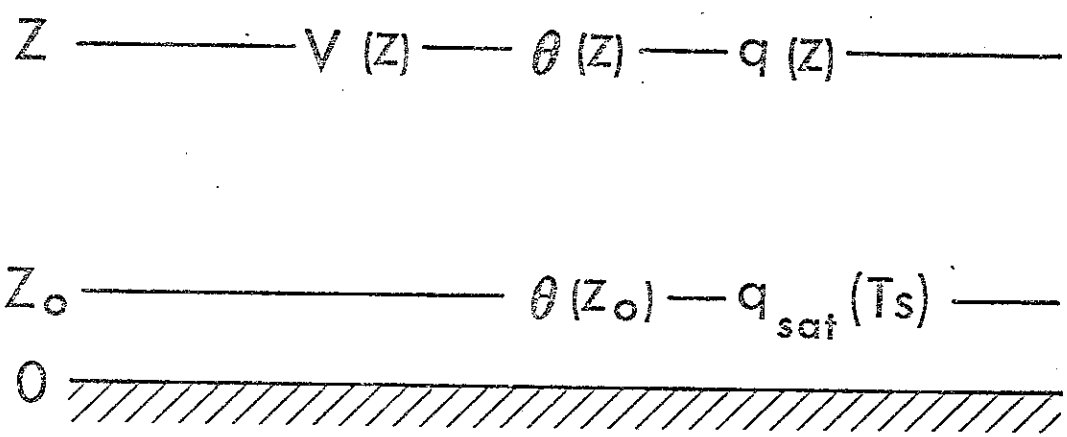

Fig. 5.2 Surface layer. Z_o, the roughness length; Z, the reference level; $q_{sat}(T_s)$, the saturation mixing ratio for the surface temperature T_s.

The soil heat conduction, H_{soil}, is (figure 5.3).

$$G = \frac{K_s \cdot C_s \cdot \rho_s}{\left(Z_{g,1} - \frac{d_s}{2}\right)} \left(T_s - T_{g,1}\right) \qquad (5.9)$$

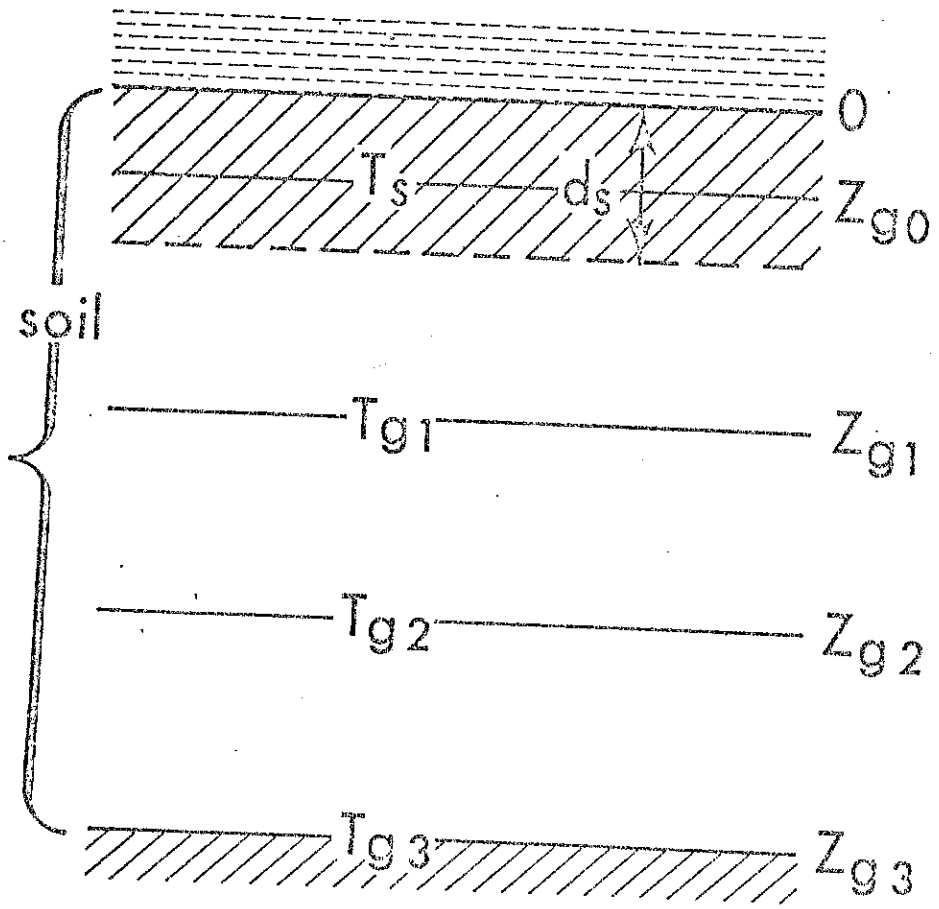

Fig. 5.3 Subsurface three-layer model. T_s is the surface temperature; $T_{g,1}$, $T_{g,2}$ and $T_{g,3}$ are the soil temperatures at levels of $Z_{g,1}$, $Z_{g,2}$ and $Z_{g,3}$.

Eq. (5.4) is solved by marching calculation (implicit-scheme) under the condition that $\theta(z)$, $q(z)$, $V(z)$, $R_S\downarrow$, $R_L\downarrow$ for the atmosphere and $T_{g,1}$, β for the soil are given.

5.2 Heat balance over land with snow/ice

Whether it snows or not or how much snow is deposited on the ground are treated as separate issues. We are only concerned here with the snow melt and the prediction of surface temperature.

For this reason, if snow is not on the ground, the case does not belong to this subsection but to the last subsection.

If there is snow on the ground, we first compute a provisional surface temperature, T_S, from (5.4) with $E_X=0$. Then one of two cases can occur.

a) $T_S \leq 273.16°K$ (below or at the freezing point). There is no snow-melt, and T_S is the final surface temperature.

b) $T_S > 273.16°K$ (above freezing). The snow is melted to either the degree that $T_S \to 273.16°K$ or the snow is melted entirely.

First, recalculate H_{soil} as

$$L_f \cdot E_x = R_n - H_o - L \cdot E_o + H_{soil} \qquad (5.10)$$

with $T_S=273.16°K$. Then

$$S_{max} = E_x \cdot \Delta t \qquad (5.11)$$

represents the maximum depth of snow (in water equivalent per unit area that can be melted by lowering the ground temperature T_S to freezing point. Compare S_{max} with the existing snow depth (per unit area), S. If $S \gg S_{max}$, then

$$S(\text{after}) = S(\text{before}) - S_{max} \tag{5.12}$$

$$T_s(\text{after}) = 273.16\,^{\circ}K \tag{5.13}$$

and if $S \leq S_{max}$, then

$$E_x(\text{part}) \cdot \Delta t = S(\text{before}) \tag{5.14}$$

$$S(\text{after}) = 0 \tag{5.15}$$

Predict new T_s, based on

$$\frac{C_s \cdot \rho_s \cdot d_s \left[T_s(\text{after}) - 273.16\,^{\circ}K \right]}{\Delta t} = \left(R_n - H_o - L \cdot E_o \right)_{273\,^{\circ}K} + H_{soil}(273) - L_f \cdot S / \Delta t \tag{5.16}$$

S is the water-equivalent depth of snow (when it is melted to water.) The apparent snow depth in the state of solid is multiplied by 10.

5.3 Balance over sea

A water body has large heat capacity, so that it serves to moderate the extreme atmospheric temperature, to retain the absorbed solar energy, and afterwards to release a large amount of water vapor.

The heat balance equation is similar to eq. (5.4), except that G should be the flux into water. The ocean treated in this manual is, however, the so-called fixed ocean. So the heat balance equation is not used. Two cases can be considered, i.e., sea without ice and sea-ice.

a) Sea without ice

The heat budget equation is not treated. The surface temperature is

specified by prepared data, i.e.,

$$T_s = T_{sea\ surf} \tag{5.17}$$

$T_{sea\ surf}$ is the climatological values (Alexander and Mobley, 1976), which vary with space and time.

The sensible and latent heats are given by

$$H_o/c_p = -\rho C_H \cdot [\theta(z) - \theta(z_o)] \tag{5.18}$$

$$E_o = -\rho C_H \cdot [q_s(z) - q_{sat}(T_s)] \tag{5.19}$$

b) Sea ice

The ice limits are specified by climatological normals, which vary in time and space (Alexander and Mobley, 1976). In the polar regions inside of the ice limit the sea surface temperature is fixed equally to -2°C.

The temperature at the interface between sea-ice and air is determined by the heat budget equation as

$$\frac{\partial C_{ice}\rho_{ice}d_{ice}\cdot T_{ice}}{\partial t} = R_n - H_o - L\cdot E_o - L_f\cdot E_x + \lambda_{ice}\frac{\partial T_{ice}}{\partial z} \tag{5.20}$$

where C_{ice}, ρ_{ice}, d_{ice} and λ_{ice} are the quantities associated with ice.

d_{ice} is specified uniformly as 2 meters. In reality, it is thicker than 2 meters (see Footnote I).

λ_{ice} = 2.03 W/m.deg is used. This value is for pure ice (see Footnote II).

Footnote I:

The most important in the energy balance over arctic sea ice is the correct specification of the sea ice thickness. Presently the model uses 2 meters everywhere there is sea ice. But the ice near the Canadian archipelago is always as thick as 6 meters; and average thickness is 3 ~ 4 meters (figure 5.4). The heat flux would be cut in half over half the area extent of the arctic ice cap if climatological or observed sea ice thicknesses are used.

Fig. 5.4

Footnote II:

Presently, the flux of heat through sea ice is computed using the conductivity λ_{ice}, for pure ice. λ_{ice} is, however, a function of salinity and snow depth.

Untersteiner gives the following relationship for the conductivity of sea ice as a function of salinity S:

$$\lambda_{ice} = \lambda_{oice} + \mu s/(T_s - 273)$$

where

$\mu\beta$ = .117 W m^2/Kg

s = salinity in Kg/m^3

λ_{oice} = conductivity of pure ice 2.03 W/m°K

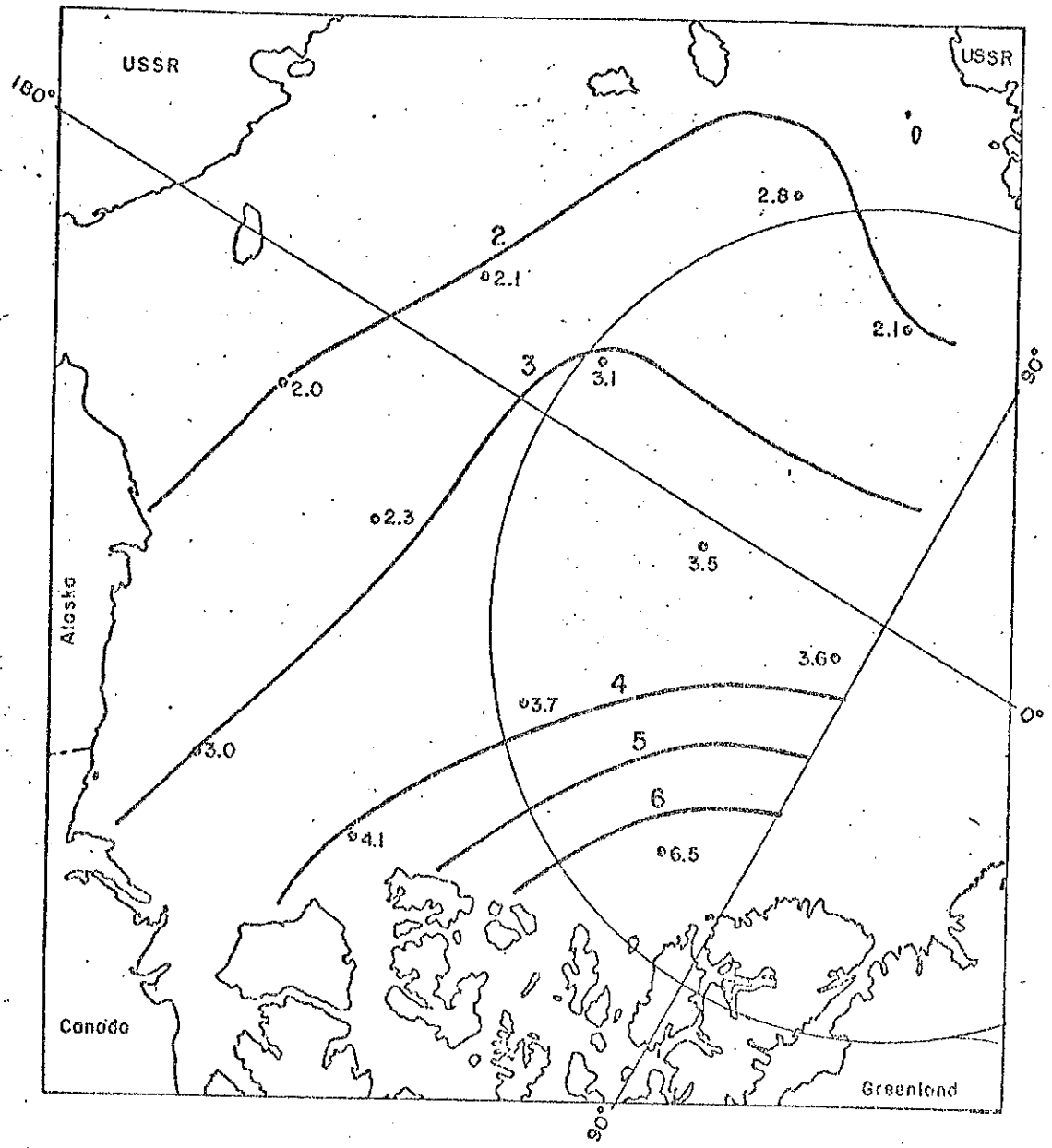

Fig. 5.4 Observed ice thickness values obtained from submarine sonar data. Units are meters (after Hibler, 1979).

Salinity is a function of ice thickness; some selected values are: 7.3 for 0.4 meters and 5.2 for 1.0 meters of ice. Clearly, for thickness of 2 to 6 meters, salinity is of minor importance.

The combined snow and sea ice effective conductivity, λ_{eff}, can be shown to be given by the following expression

$$\lambda_{eff} = (\lambda_{ice}\lambda_{snow}H_{ice})/(\lambda_{snow}H_{ice} + \lambda_{ice}H_{snow})$$

where,

$\lambda_{ice}, \lambda_{snow}$ = sea ice and snow heat flux conductivities respectively

H_{ice}, H_{snow} = sea ice and snow thickness respectively

The snow depth H_{snow} over the arctic ice cap is at best 20 cm which is much smaller than the sea ice thickness H_{ice}. Therefore, in regions where $H_{snow} << H_{ice}$, the effective snow-ice conductivity λ_{eff} reduces to that of sea ice λ_{ice}. This occurs when the sea ice thickness is greater than one meter.

6. Land Surface Conditions

To those living on the surface, the conditions described in this section are of a great concern, and they affect quickly the atmospheric temperature and humidity. To the large-scale atmospheric circulation also, these conditions provide substantial effects on the time scale of 20 days and beyond.

6.1 Determination of soil moisture (SM)

Figure 6.1 illustrates the hydrologic process over land surface and the immediate subsurface. The conservation relation of water mass (SM) is written by

$$Z_r \frac{\partial w}{\partial t} = P - E_o - r_f - P_r \qquad (6.1)$$

where w is the volumetric soil moisture content (i.e., volume of water/total volume) (in units of gr. cm^{-3}) Z_r is the root-zone depth, P is the rate of rainfall (gr. $cm^{-2}.s^{-1}$), E_o is the rate of evaporation (gr.$cm^{-2}s^{-1}$), r_f is the rate of runoff (surface runoff), and P_r is the rate of percolation to water table (gravitational flux of moisture). This equation is applied to the layer of vegetation root-depth, Z_r. Hydrologists consider another layer, to which the water goes through P_r.

Fig. 6.1

In this manual, following the version of Manabe (1969), the second layer is not considered; i.e., $P_r=0$. Accordingly $Z_r.w=W$ is used in (6.1).

The evapotranspiration, $E_T(=E_o)$ depends on SM, so

$$E_T = \beta \cdot E_{pot} \qquad (6.2)$$

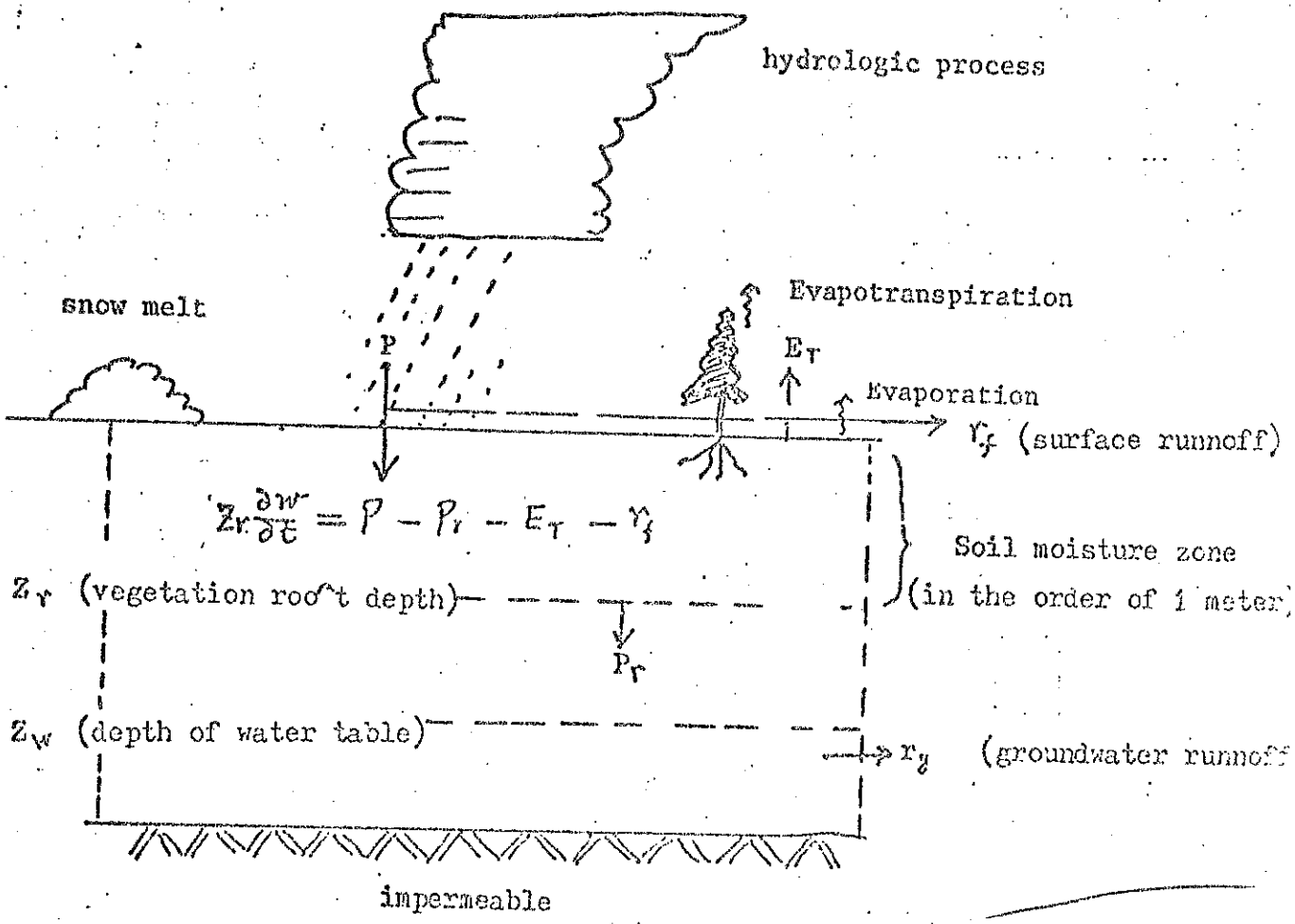

Fig. 6.1 Hydrological processes.

where E_{pot} is the potential evaporation, which is defined as the evaporation that occurs from a freely transpiring surface or from a wet bare surface. E_{pot} is a key variable, which will be discussed later.

The ground wetness, β, is specified as

$$\beta = \begin{cases} 1 & \text{if } W \geq W_k \\ W/W_k & \text{if } W < W_k \end{cases} \qquad (6.3)$$

where

$$W_k = 0.75 \times W_{FC} \qquad (6.4)$$

and W_{FC} is the "field capacity of soil moisture," i.e., the upper limit of water that can be stored in soil W_{FC}=15 cm (or W_k=11.25 cm) is in current use (see figure 6.2a). Eagleson (1981) recommends that the soil moisture storage capacity should be estimated on the bases of root-zone depth Z_r and soil porosity n rather than "outmoded concept of field capacity." Figure 6.2b is the relation of E_T/E_{pot} and $W/n(=\theta/n$ in the figure) by Eagleson (1982), which was modified from the original diagram of Lowry (1959). In practice, however, in order to follow the Eagleson's suggestion, it is needed to have maps of Z_r and n over the global continents. Note that β is referred to as the "evaporation efficienty," "the ground wetness," "the availability of soil moisture," or "the degree of shortage of water."

Fig 6.2

Budyko recommends using field capacities ranging from 15 g/cm^2 in winter to 30 g/cm^2 in summer over deserts, 20 g/cm^2 in forested regions in early spring to 15 g/cm^2 in summer, and 17 g/cm^2 in spring to 12 g/cm^2 in summer over forested steppe regions.

Based on the equations (6.1)-(6.3) the SM and the r_f (runoff) are

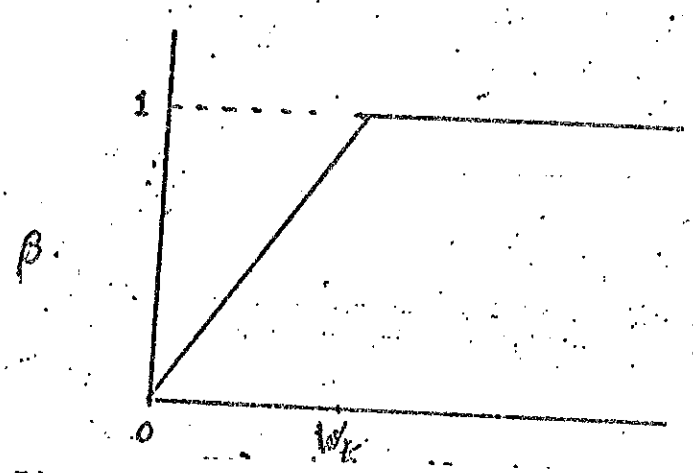

Fig. 6.2a β vs W (volumetric soil moisture, $W = Z_r.w$).

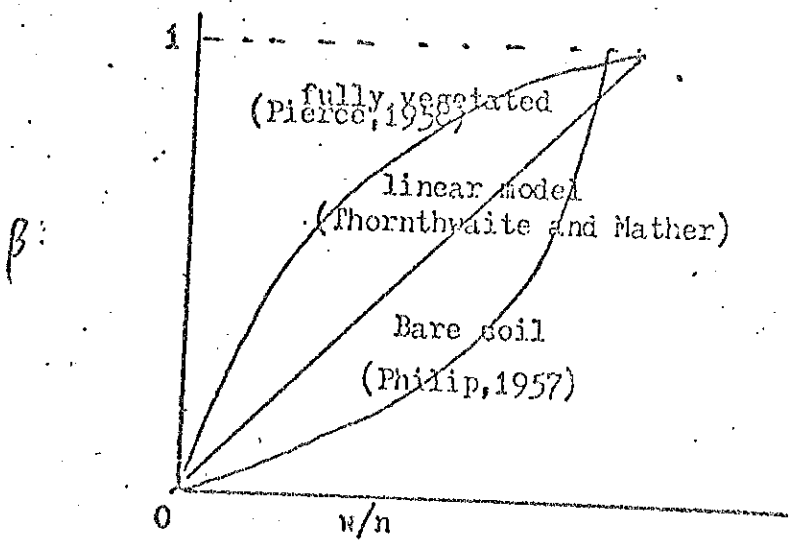

Fig. 6.2b β ($=E_T/E_{pot}$) vs w/n. n is the porosity (after Lowry, 1959).

determined. First calculate the rate of snow melt, M_e,

$$M_e = E_x / L_f \cdot \Delta t \qquad (6.5)$$

a) The case of no snow

If $M_e \leq 0$, there is no snow melt

$$\text{If } W = W_{FC} \text{ and } P > E_o,$$

$$\frac{\partial W}{\partial t} = 0 \text{ and } r_f = P - E_o . \qquad (6.6)$$

$$\text{If } W < W_{FC},$$

$$\frac{\partial W}{\partial t} = P - E_o \text{ and } r_f = 0 . \qquad (6.7)$$

b) The case of snow melt

If $M_e > 0$, there is snow melt

If $W < W_{FC}$,

$$\frac{\partial W}{\partial t} = M_e + P \qquad (6.8)$$

If $W = W_{FC}$

$$\frac{\partial W}{\partial t} = 0 \text{ and } r_f = M_e + P \qquad (6.9)$$

snow amount:

$$\frac{\partial S}{\partial t} = S_F - E_o - M_e \qquad (6.10)$$

where $E_o = E_T$, and S_F is the rate of snowfall.

Determination of evapotranspiration

The evapotranspiration consists of three major components. One is the evaporation from the bare soil. The second and the third are the trans-

piration from the grass covered land and from dense forest (tall tree) land, respectively.

In this manual, two versions of the calculation will be described. The first one has been conventionally used in GFDL (Manabe, et al. 1965); the second one is the Priestley-Taylor (1972) method. Version I has not been well tested against observation, as an individual formula, and yet it has been employed for many years. The total evaporation over the ocean, as revealed in GCM experiment in Manabe et al. (1974), agrees remarkably well with the Budyko's estimate on the climatology. Version II was derived by Priestley and Taylor (1972), but somewhat different form was proposed by Penman (1948) and McIlroy (according to Davies and Allen, 1973) (see Footnote II). It is popular and was validated by observation. However, this formula is only valid for the low grass cover, bare soil, and ocean.

In the following, E_{pot} will be discussed, and the final evapotranspiration is given by $E_o = \beta \cdot E_{pot}$.

Version I

As described in eq. (5.6)

$$L \cdot E_{pot} = -L \cdot \rho \cdot C_H \cdot [\, q(z) - q_{sat}(T_s) \,] \qquad (6.11)$$

The current E-physics uses Versin I.

Version II

$$L \cdot E_{pot} = 1.26 \, \frac{\Delta}{\Delta + \gamma} \, (R_n - G_T) \qquad (6.12)$$

where $S = \frac{\partial q_{sat}}{\partial T}$, $\gamma = c_p/L$, and 1.26 is an empirical constant (Priestley and Taylor, 1972). G is normally very small, so it can be neglected. (Figure 6.3) See Footnote I for derivation of the formula.

Fig. 6.3

Footnote I:

The ratio of L E_o and H_o (reverse of B_o) is written for the case of saturated surface as

$$\frac{L \cdot E_o}{H_o} = \frac{L}{c_p} \frac{q(T) - q_{sat}(T_s)}{T - T_s} \qquad (F.1)$$

Then if T is close to T_s, eq. (F.1) is treated by Taylor expansion as

$$\frac{L \cdot E_o}{H_o} \doteq \frac{L}{c_p} \frac{\partial q_{sat}}{\partial T} = \frac{s}{\gamma} \qquad (F.2)$$

where

$$s = \frac{\partial q_{sat}}{\partial T} , \quad \gamma = c_p/L \qquad (F.3)$$

Therefore

$$L \cdot E_o = \frac{s}{s+\gamma} (L \cdot E_o + H_o) \qquad (F.4)$$

or

$$L \cdot E_o = \frac{s}{s+\gamma} (R_n - G) \qquad (F.5)$$

R_n is the net radiation, and G is the heat flux into the soil (or ocean). However, this is only valid for the saturated surface, and in general, it is written as

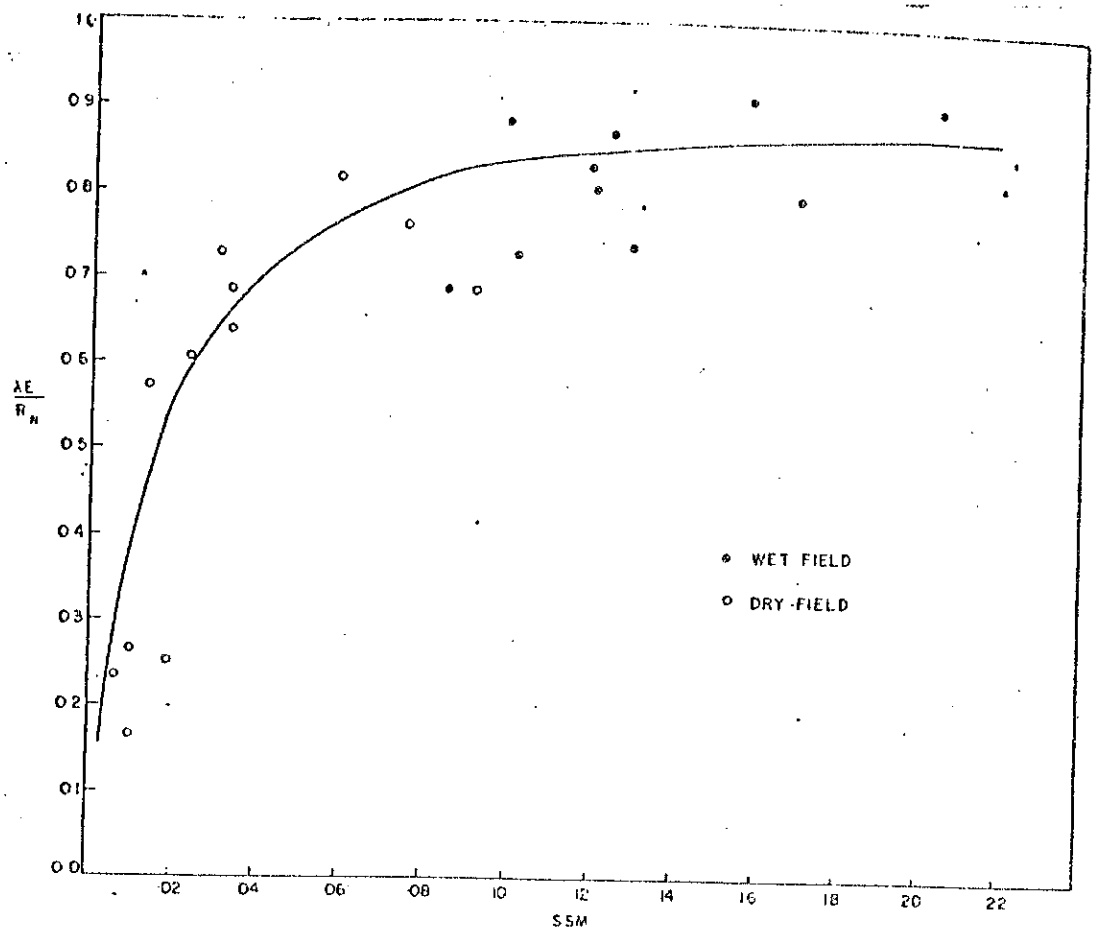

Fig. 6.3 Variation of evaporation, expressed as $L.E_0/R_n$, with surface soil moisture (SSM) (after Davies and Allen, 1973).

$$L \cdot E_o = \alpha \cdot \frac{\Delta}{\Delta+\gamma}(R_n - G) \qquad (F.6)$$

α is empirically determined (=1.26). See also Figure 6.3.

$B_o = H_o/L.E_o$ is written as (Priestley and Taylor, 1972)

$$\frac{1 - 1.26\ \frac{\Delta}{\Delta+\gamma}}{1.26\ \frac{\Delta}{\Delta+\gamma}} \qquad (F.7)$$

which is a function of only temperature. Figure 6.4 shows that the ratio indeed depends on temperature.

Fig. 6.4

Footnote II:

Penman (1948) proposed a formula, which is reproduced here, using eqs. (6.11) and (6.12) as

$$L \cdot E_{pot} = \frac{\Delta_e}{\Delta_e + \gamma} \cdot eq\ (6.12) + \frac{\gamma}{\Delta_e + \gamma} \cdot eq\ (6.11)$$

$$= \frac{1}{\Delta_e + \gamma}\left[\Delta_e \cdot 1.26\ (R_n - G) - \gamma \cdot L \cdot \rho \cdot C_H\ (q(z) - q_{sat}(T_s))\right]$$

(F.8)

where Δ_e is the slope of the saturated vapour pressure-temperature curve, i.e., $\frac{de_{sat}}{dT}$, and γ is psychrometric constant $\gamma = c_p.p/0.622.L$. See Brutsaert (1982) for the derivation. The original form of the second term in (F.8) is, instead of eq. (6 11), $E_A \propto (e_{sat}-e)$, e being the vapor pressure.

Footnote III:

Mintz (1982) shows the large difference of evaporation between short

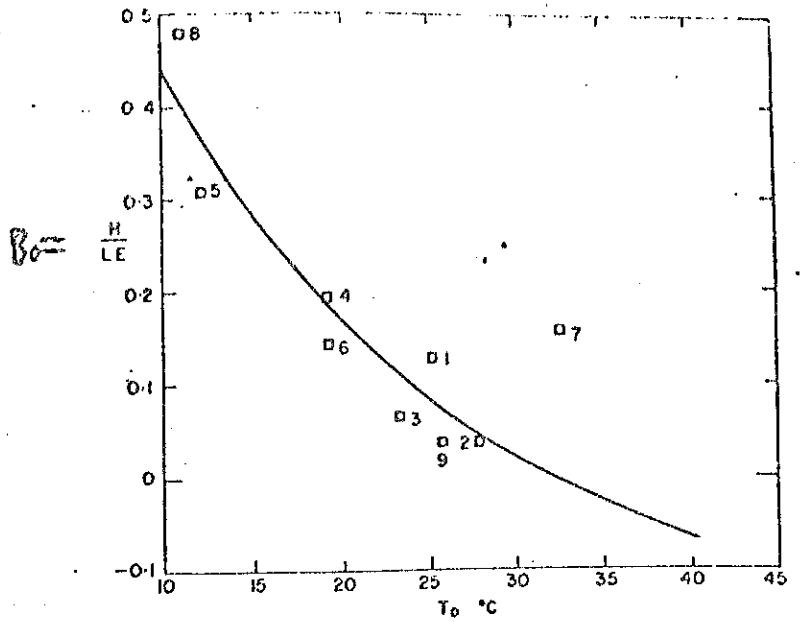

Fig. 6.4a Ratio of H to LE plotted against temperature. Values for (1) Indian Ocean (University of Washington), (2) Indian Ocean (CSIRO D_m 1/62), (3) Indian Ocean (CSIRO G. 4/62), (4) Lake Eucumbene, (5) CSIRO lysimeter, (6) University of Wisconsin lysimeter, (7) fluxation, (8) Wangara, and (9) Atlantic Ocean are plotted (after Priestley and Taylor, 1972).

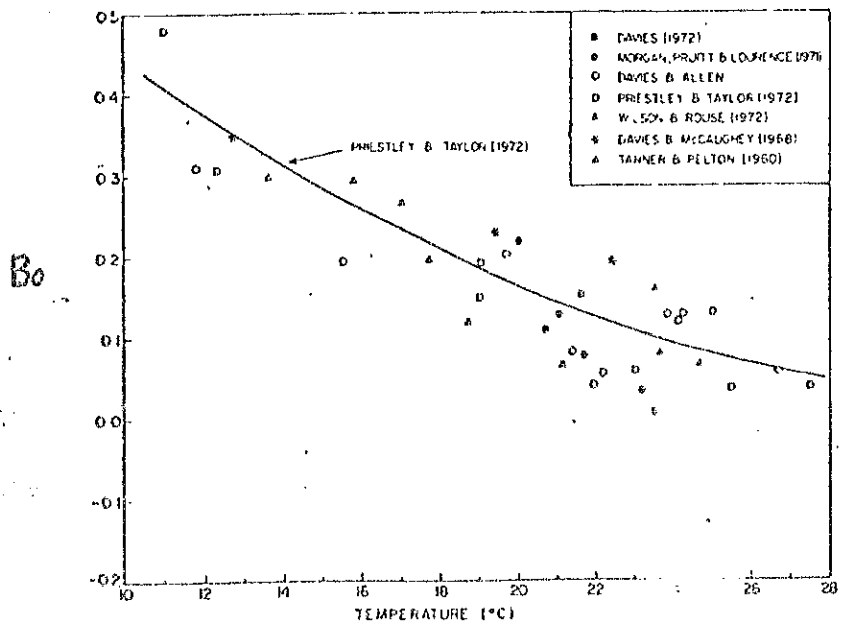

Fig. 6.4b Variation of B_0 for a moist surface with air temperature (after Davies and Allen, 1973).

and tall vegetation. Tall vegetation has good ventilation, because of the elevated position of the trees' top and the large volume of leaves. As a result, the rate of transpiration is much larger than the counterpart of low vegetation. It is interesting to note that the forest removes sensible heat from the boundary layer, and consequently, H_0 is negative, which means that B_0 is negative.

6.3 Soil heat conduction

The diurnal variability of surface temperature could be very large, particularly in summer sand desert. In this connection, the soil heat conduction serves to alleviate the extreme temperature appreciably (Bhumralkar, 1975, mentioned that the diurnal range of 56°C is observed in Africa, whereas a numerical model can give even 70°C without the effect of soil heat conduction.).

The heat conduction equation is written as

$$C_s \cdot \rho_s \frac{\partial T_g}{\partial t} = \lambda \cdot \frac{\partial^2 T_g}{\partial z^2} \qquad (6.14)$$

where λ is the thermal conductivity

$$\lambda = c_s \rho_s k_s \qquad (6.15)$$

K_s: thermal diffusivity

C_s: specific heat

ρ_s: bulk density of soil

$\rho_s \cdot C_s$: heat capacity

$$H_{soil} = -\left(\rho_s \cdot C_s \cdot K_s \frac{\partial T}{\partial z}\right)_{z=0} \qquad (6.16)$$

In this manual, the heat capacity is a function of the ground wetness, β, and the form is tentatively

$$\rho_s C_s = (0.254 + \beta)$$

For $\beta = 0$,

$\rho_s = 1.5$ g cm^{-3}

$C_s = 0.32$ cal.g^{-1},deg^{-1}

$K_s = 3.0 \times 10^{-3}$ cm^2.s^{-1}.

E-physics model contains three soil levels (figure 6.5); 1st, 2nd, and 3rd are at the depths of 10, 50 and 500 cm, respectively (Delsol et al. 1971). The temperature at the 0th level (2.5 cm) corresponds to the surface temperature, i.e., $T_{g.o} = T_s$. The lowest boundary temperature $T_{g.3}$ is imposed by the annual mean atmosphere temperature, which changes in space but not in time.

Fig 6.5

Fig. 6.6 shows the seasonal fluctuations of the ground and underground temperature at Barrow, Alaska. The temporal shift of the temperature maxima and minima with depth is noted. For common soil, the diurnal temperature wave does not penetrate below 50 cm, and the annual wave does not go too much beyond 5 meters.

Fig. 6.6

6.4 Emissivity and albedo

The emissivity and albedo are the parameters related to radiation.

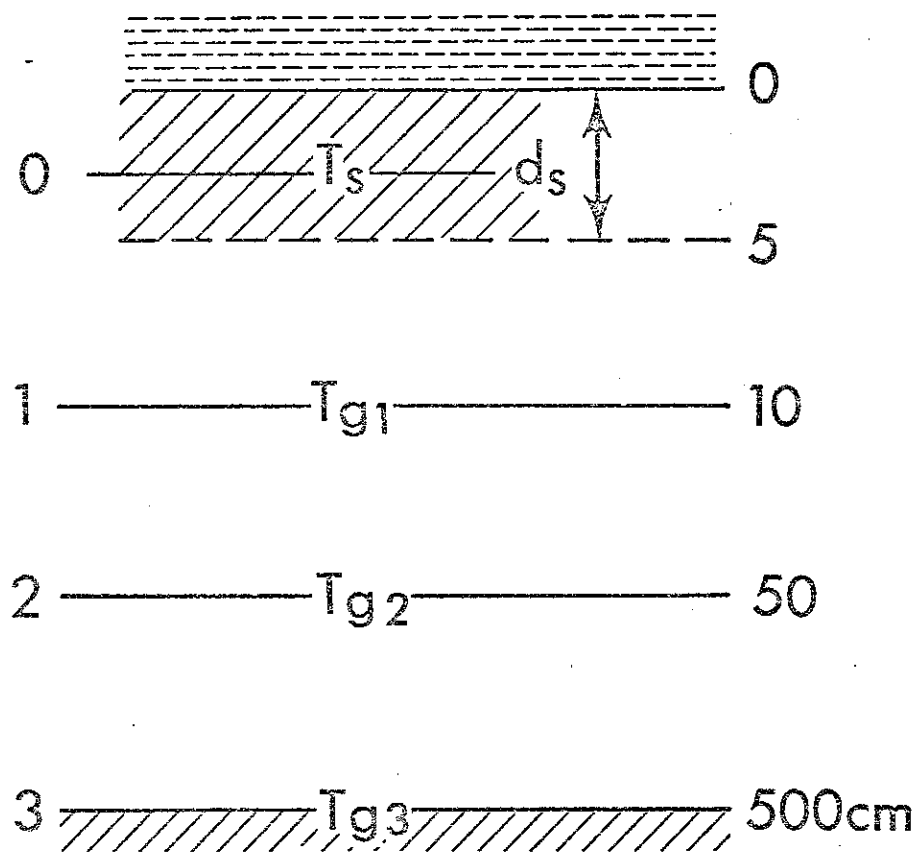

Fig. 6.5 Subsurface layers.

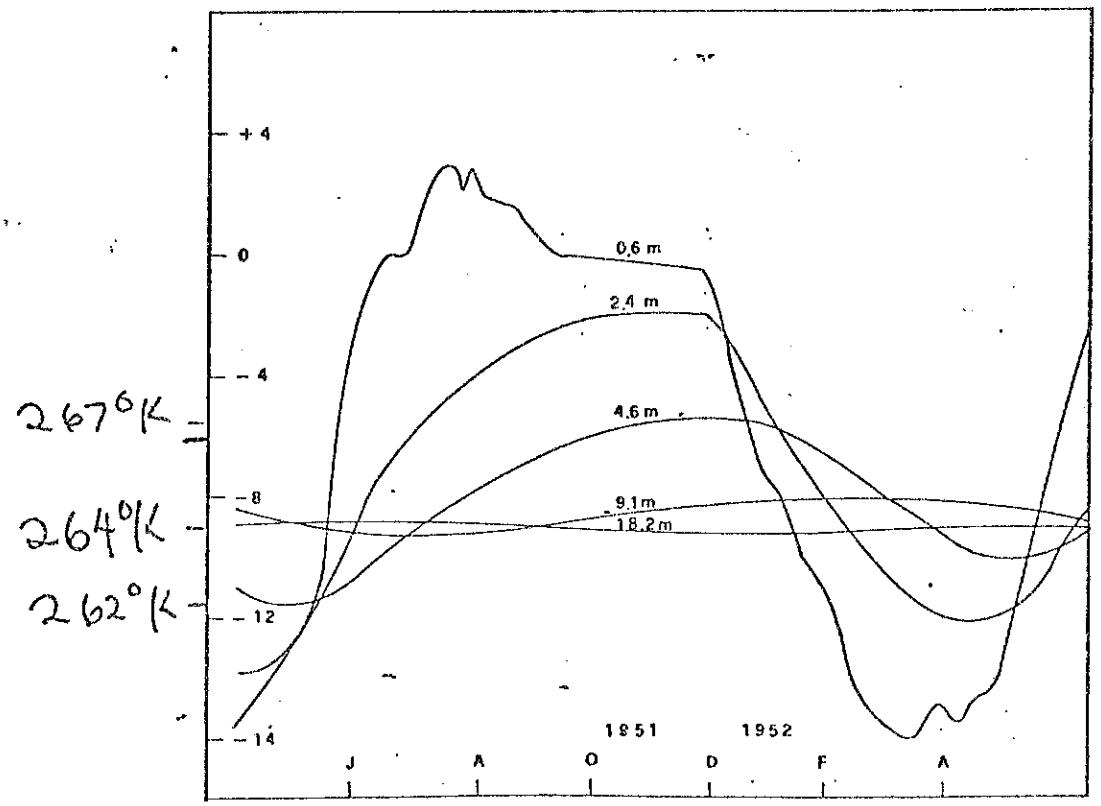

Fig. 6.6 Seasonal variations of temperature with depth measured in Barrow, Alaska (after Cooke and Doornkamp, 1977).

They vary depending on the type of land surface, snow/ice cover, and soil moisture.

Concerning the soil moisture, a discussion was given in the previous subsection. The snow/ice cover is another variable, which affects the monthly or seasonal variability of atmospheric circulation. The climatological monthly mean distribution of snow/ice is prescribed as an initial condition in forecasts. Eventually it will be replaced by the observed snow/ice cover, taking the satellite snow dta. Figure 6.7 is the climatological mean of the snow boundary for January (Wiesnet and Matson, 1979).

Fig. 6.7

a) Emissivity

The emissivity changes in measureable amount with soil moisture (Edgerton et al. 1968). For example, $\varepsilon \sim 0.85 \sim 0.95$ for dry soil, $0.4 \sim 0.8$ for moist soil. ε decreases by 0.01 for an increase of soil moisture by one percentage unit in the range of $10 \sim 20\%$ soil moisture.

depends on other factors too. Namely, smooth surfaces usually have lower emissivity than rough surfaces (Edgerton, 1970)

Dense vegetation	$\varepsilon = 0.95$
Sandstone	0.88
Granite	0.87
Basalt	0.83
Olivine	0.82
Dolomite	0.80

However, in the current E-physics,

$$\varepsilon = 1.00 \qquad (6.20)$$

is used.

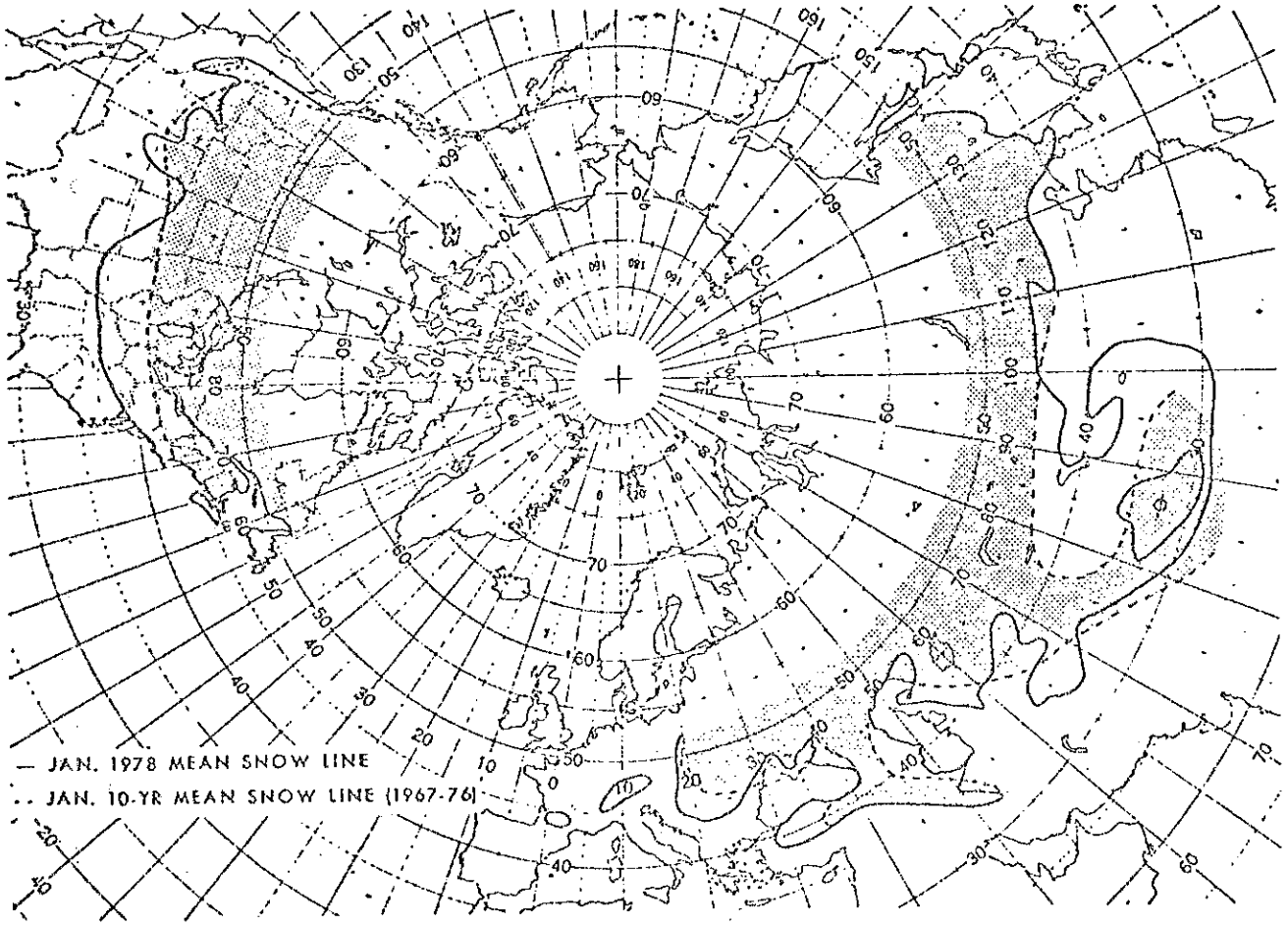

Fig. 6.7 Northern Hemisphere January 1978 mean snow line versus January 10-year mean snow line. Due to lack of sufficient solar illumination for satellite visible data, the snow line is terminated at 52°N (after Wiesnet and Matson, 1979).

b) Albedo

The surface albedo, a, is used in eq. (5.1). The global average is 0.17 or 17% with ± 25% uncertainty (Robock, 1980). The land albedo map publsihed by Posey and Clapp (1964) is now widely used, in which six different land surface characteristics are specified. Kung et al (1964) conducted a detailed study of land albedo distribution over the United States using aircraft measurements.

The general approach of specifying land albedo in a GCM is as follows. First, the background albedo is defined for all lands of the world, depending upon the land surface characteristics, such as forests, tundra or desert. This albedo is supposed to be for clear sky and to be free from snow/ice cover and for the climatologically normal soil moisture. Secondly, the effect of snow/ice cover as well as the anomaly component of soil moisture are superposed on the background albedo.

This is in current use in E-physics (Holloway and Manabe, 1971). It is heuristically assumed that the albedo changes in proportion to $\sqrt{S}$, if the snow depth, S, is less than 1 cm (water-equivalent depth) (10 cm in apparent snow depth). When S exceeds 1 cm, the albedo becomes saturated. The background albedo, a_g is taken from Posey and Clapp (see figure 6.8). fig. 6.8

Therefore

$$a = \begin{cases} a_g + \sqrt{S}\,(a_s - a_g) & \text{if } S < 1 \text{ cm} \\ a_s & \text{if } S \geq 1 \text{ cm} \end{cases} \qquad (6.21)$$

where $a_s = 0.60$.

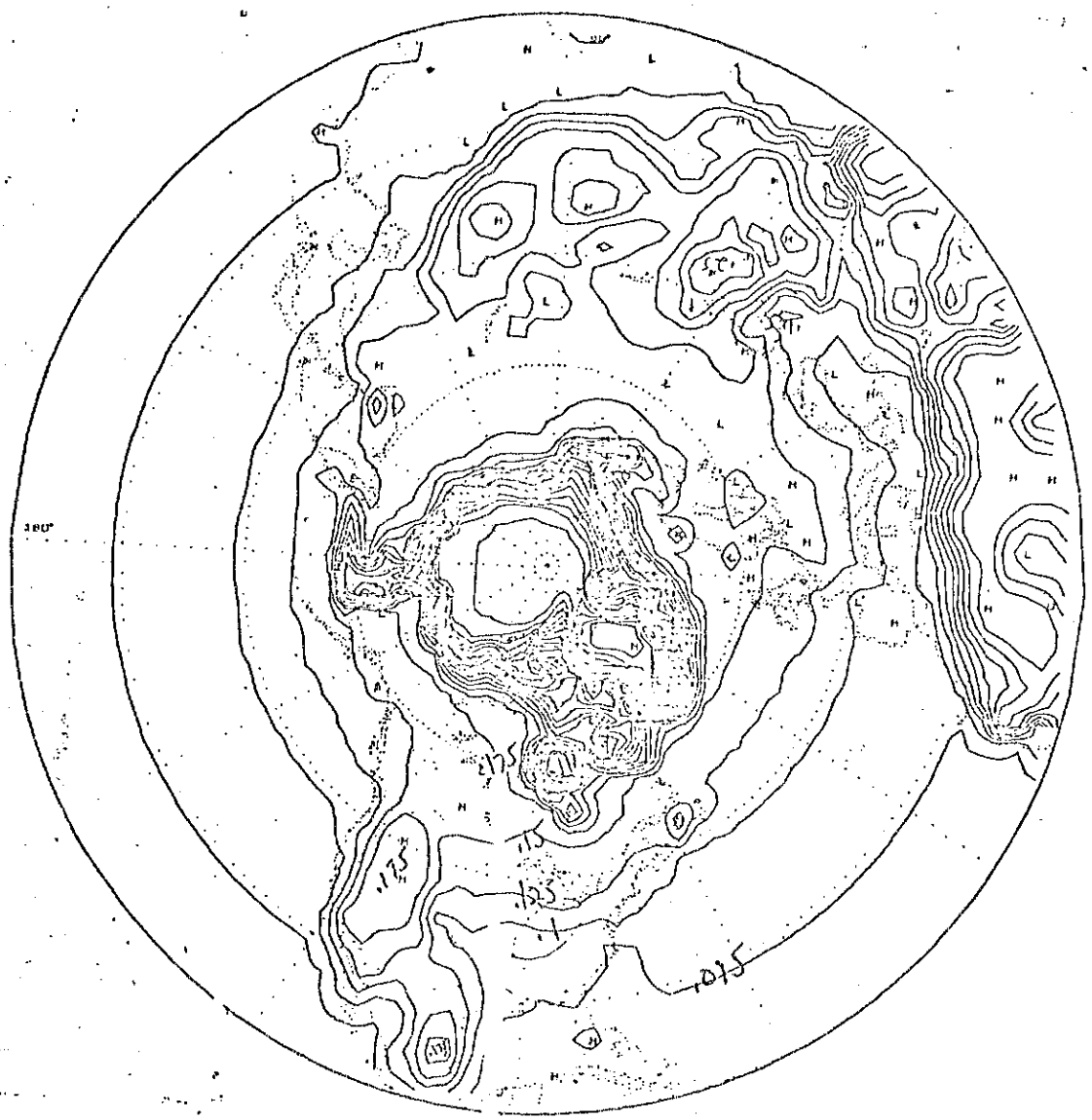

Fig. 6.8 Background albedo based on Posey and Clapp's atlas.

7. Sea Surface Condition

In ocean fixed models, the treatment of sea condition is simple.

7.1 Sea surface temperature (SST)

As mentioned in section 5.3, the SST is specified as a function of space and time. The value could be the climatological normal, or the real sea temperature, which consists of the climatology and anomaly.

In the current model, the climatology by Alexander and Mobley (1976) is employed. The original data are given as the monthly normals with their centers at the middle of the month. Therefore, the input data of SST are interpolated in time from the original monthly averages, using Fourier series expansion method.

Fig. 7.1

7.2 Emissivity and albedo

a) Emissivity

The surface emissivity ε in eq. (5.1) is given by

$$\varepsilon = 0.4 \tag{7.1}$$

over continuous liquid water surface.

b) albedo

Two cases occur.

b-1 sea water - The sea surface albedo is specified as a function of the cosine of the zenith angle based on the measurement of Payne (1972).

b-2 sea ice/snow

If $T_S < 0°C$ and snow ≤ 0

$$a = 0.50 \tag{7.6}$$

and if snow ≥ 0

$$\begin{cases} a = 0.75 & \text{for latitude} \geq 70° \\ a = 0.60 & \text{for latitude} < 70° \end{cases} \qquad (7.7)$$

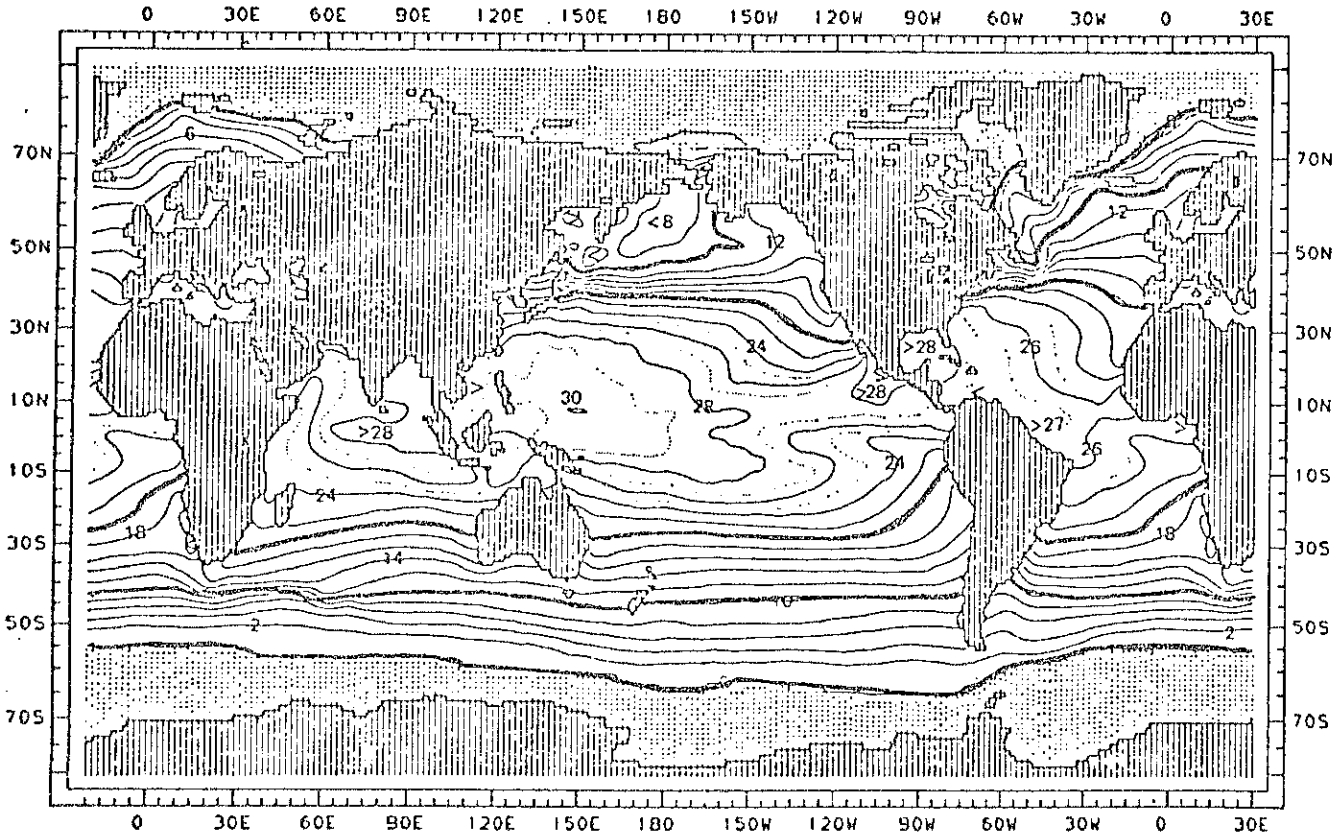

Fig. 7.1 July average ocean surface temperature (°C) and ice-pack distribution (broken vertical hash marks). Temperature isopleth interval is 2°C, with intermediate isotherms in low latitudes designated by dotted lines (after Alexander and Mobley, 1976).

References

Alexander, R. C. and R. I. Mobley, 1976: Monthly average sea-surface temperature and ice-pack limits on a 1° global grid. Mon. Wea. Rev., 104, 143-148.

Arakawa, A., 1972: Design of the UCLA general circulation model. Tech. Rep. 7, p. 103. Dept. Meteor., Univ. of Calif., Los Angeles.

Baumgartner, A. and E. Reichel, 1975: The World Water Balance. Elsevier Sci. Pub. Co., Amsterdam and NY, 178 pp.

Benoit, R., 1977: On the integral of the surface layer profile-gradient functions. J. Appl. Met., 16, 859-860.

Blackadar, A. K. 1962: The vertical distribution of wind and turbulent exchange in a neutral atmosphere. J. Geophys. Res., 67, 3095-3102.

Bleck, R., 1977: Numerical simulation of lee cyclogenesis in the Gulf of Genoa. Mon. Wea. Rev., 105, 428-445.

Bhumralkar, C. M., 1975: Numerical experiments on the computation of ground surface temperature in an atmospheric general circulation model. J. Appl. Meteor., 14, 1246-1258.

Brutsaert, W. H., 1982: Evaporation Into the Atmosphere. D. Reidel Publ. Co., 299 pp.

Budyko, M. I., 1974: Climate and Life. Academic Press, NY., 508 pp.

Businger, A., J. C. Wyngaard, Y. Izumi, and E. F. Bradley, 1971: Flux-profile relationships in the atmospheric surface layer. J. Atmos. Sci., 28, 181-189.

Carson, D. J., 1973: The development of a dry inversion-capped convectively unstable boundary layer. Quart. J. Roy. Meteor. Soc., 99, 450-467.

_____, and P. J. R. Richards, 1978: Modelling surface turbulent fluxes in stable conditions. Boundary-Layer Meteor., 14, 67-81.

Charney, J. G., W. J. Quirk, S. Chow and J. Kornfield, 1977: A comparative study of the effects of albedo change on drought in semi-arid regions. J. Atmos. Sci., 34, 1366-1385.

Charnock, H., 1955: Wind stress on a water surface. Quart. J. Roy. Met. Soc., 81, 639-640

Clarke, R. H. 1970: Recommended methods for the treatment of the boundary layer in numerical models. Austr. Met. Mag., 18, 51-71.

_____, 1970a: Observational studies in the atmospheric boundary layer. Quart. J. Roy. Met. Soc., 96, 91-114.

_____, J. H. Ferziger and W. C. Reynolds, 1979: Evaluation of subgrid scale models using an accurately simulated turblent flow. J. Fluid Mech., 91, Part 2, 1-16.

Cogley, J. G., 1979: The albedo of water as a function of latitude. Mon. Wea. Rev., 107, 775-781.

Corby, G. A., A. Gilchrist, and R. L. Newson, 1972: A general circulation model of the atmosphere suitable for long period integrations. Quart. J. Roy. Meteor. Soc., 98, 809-832.

Cressman, G. P., 1960: Improved terrain effects in barotropic forecasts. Mon. Wea. Rev., 88, 327-342.

Davies, J. A. and C. D. Allen, 1973: Equilibrium, potential and actual evaporation from cropped surfaces in southern Ontario. J. Appl. Meteor., 12, 649-657.

Deardorff, J. W., 1971: On the magnitude of the subgrid scale eddy coefficient. J. Comput. Phys., 7, 120-133.

_____, 1973: The use of subgrid transport equations in a three-dimensional model of atmospheric turbulence. Transactions of the ASME, Paper No. 73-FE-21., 1-10.

_____, 1973: The use of subgrid transport equations in a three-dimensional model of atmospheric turbulence. J. Fluid Engin., 429-438.

_____, 1978: Efficient prediction of ground surface temperature and moisture, with inclusion of a layer of vegetation. J. Geophys. Res., 83, 1889-1903.

Delsol, F., K. Miyakoda, and R. H. Clarke, 1971: Parameterized processes in the surface boundary layer of an atmospheric circulation model. Quart. J. Roy. Met. Soc., 97, 181-208.

Dyer, A. J., 1974: A review of flux-profile relationships. Boundary Layer Meteor., 1, 363-372.

_____, and B. B. Hicks, 1970: Flux-gradient relationships in the constant flux layer. Quart. J. Roy. Meteor. Soc., 96, 715-721.

Eagleson, P. S., 1981: Dynamic hydro-thermal balances at macroscale. Proceedings of JSC Study Conference on Land Surface Processes in Atmospheric General Circulation Models. World Meteorological Organization, 289-357.

Edgerton, A. T., Mandl, R. M., et al. 1968: Passive microwave measurements of snow, soils, and snow-ice-water systems. Technical Report No. 4, SGD 829-6, 15 Feb, 1968, Space Division, Aerojet-General Corporation, El Monte, Calif.

Fennessy, M. J., and Y. C. Sud, 1983: A study of the influence of soil moisture on future precipitation. NASA Tech. Memo. 85042, Laboratory for Atmospheric Science. Global Modeling and Simulation Branch, NASA,

Goddard Space Flight Center, Greenbelt, MD 20771, 123 pp.

Fiedler, F. and H. Panofsky, 1972: The geostrophic drag coefficient and the effective roughness length. Quart. J. Roy. Meteor. Soc., 98, 213-220.

Garratt, J. R., 1977: Review of drag coefficients over oceans and continents. Mon. Wea. Rev., 105, 915-929.

Grishchenko, D. L., 1959: The dependence of albedo of the sea on the altitude of the sun and disturbance of the sea surface. Tr. Glac. Geofis. Observ., 80, 32-38.

Hibler, W. D., 1979: A dynamic thermodynamic sea ice model. J. Phys. Oceanogr., 9, 815-846.

Hicks, B. B., 1976: Wind profile relationships from the "Wangara" experiment. Quart J. Roy. Met. Soc., 102, 535-551.

Holloway, J. L. and S. Manabe, 1971: Simulation of climate by a global general circulation model: I. Hydrologic cycle and heat balance. Mon. Wea. Rev., 99, 335-370.

Hoxit, L. R., 1973: Variability of planetary boundary layer winds. Dept. Atmos. Science, Colorado State Univ., Fort Collins, CO. Atm. Sci. Paper No. 199, 157 pp.

Hummel, J. R. and R. A. Reck, 1979: A global surface albedo model. J. Appl. Meteor., 18, 239-253.

Idso, S. B., R. D. Jackson, R. I. Reginato, B. A. Kimball, and F. S. Nakayama, 1975: The dependence of base soil albedo on soil water content. J. Appl. Met., 14, 109-113.

Kitaigorodski, S. A., 1973: The Physics of Air Sea Interaction. Israel

Program for Scientific Translation, Jerusalem, 237 pp.

Kondratyev, K. Ya, 1973: Radiation Characteristics of the Atmosphere and the Earth's Surface. Amerind Pub. Co., New Delhi, 580 pp.

Kung, E. C., 1963: Climatology of aerodynamic roughness parameter and energy dissipation in the planetary boundary layer of the Northern Hemisphere. Annual Report, Contract DA-36-039-AMC-00878, Dept. of Meteor., University of Wisconsin, 37-96.

_____, R. A. Bryson and D. H. Lenschow, 1964: Study of a continental surface albedo on the basis of flight measurements and structure of the earth's surface cover over North America. Mon. Wea. Rev., 92, 543-564.

_____, and H. H. Lettau , 1961: Regional and meridional distribution of continental vegetation cover and aerodynamic roughness parameters. Annual Report, Dept. Meteor., Univ. of Wisconsin, DA-36-039-AMC-00878, 37-96.

Kukula, G. J., 1976: Global variation of snow and ice content. Paper presented at COSPAR.

Leith, C. E., 1969: Two-dimensional eddy viscosity coefficients. Proceedings WMO/IUGG Symposium on Numerical Weather Prediction, Tokyo, Japan Met. Agency, 2-5.

Lenschow, D. H., 1973: Two examples of planetary boundary layer modification over the Great Lakes. J. Atmos. Sci., 30, 568-581.

_____, 1974: Model of the height variation of the turbulence kinetic energy budget in the unstable planetary boundary layer. J. Atmos. Sci., 31, 465-474.

Leonard, A., 1973: On the energy cascade in large-eddy simulations of turbulent flows. Adv. in Geophys., A18, 237.

Lettau, H. H. and B. Davidson, 1957: Exploring the Atmosphere's First Mile. Pergamon Press, 578 pp.

Lewellen, W. S. and M. Teske, 1973: Prediction of the Monin-Obukhov similarity functions from an invariant model of turbulence. J. Atmos. Sci., 30, 1340-1345.

Lilly, D. K. 1967: The representation of small-scale turbulence in numerical simulation experiments. Proceedings IBM Scientific Computing Symposium on Environmental Sciences, Thomas J. Watson Research Center, Yorktown Heights, NY, 195-210.

Lowry, W. P., 1959: The falling rate phase of evaporative soil moisture loss: a critical evaluation. Bull. Amer. Meteor. Soc., 40, 605-608.

Mahrer, Y., 1979: Prediction of soil temperatures of a soil mulched with transparent polyethylene. J. Appl. Meteor., 18, 1263-1267.

Manabe, S., 1969: Climate and the ocean circulation. I. The atmospheric circulation and the hydrology of the earth's surface. Mon. Wea. Rev., 97, 739-774.

_____, D. G. Hahn and J. L. Holloway, 1974: The seasonal variation of the tropical circulation as simulated by a global model of the atmosphere. J. Atmos. Sci., 31, 43-83.

Mellor, G. L., 1973: Analytic prediction of the properties of stratified planetary surface layers. J. Atmos. Sci., 30, 1061-1069.

_____, and H. L. Herring, 1973: A survey of the mean turbulent field closure models. AIAA Journal, 11, 590-599.

_____ and T. Yamada, 1974: A hierarchy of turbulence closure models for planetary boundary layer. J. Atmos. Sci., 31, 1791-1806. See also Corrigenda, Ibid., 34, 1482.

_____and T. Yamada, 1977: a turbulence model applied to geophysical fluid problems. Proceedings of the Symposium on Turbulent Shear Flows. The Pennsylvania state University, April, 1977, 611-614.

_____and _____, 1982: Development of a turbulence closure model for geophysical fluid problems. Rev. Geophys. Space Phys., 20, 851-875.

Melville, W. K., 1977: Wind stress and roughness length over breaking waves. J. Phys. Oceanogr., 7, 702-710.

Mintz, Y., 1982: The sensitivity of numerically simulated climates to land-surface conditions. JSC Study Conference on Land-Surface Processes in Atmospheric General Circulation Models, Greenbelt, USA, 5-10 January, 1981.

Miranova, Z. F., 1973: Albedo of earth's surface and clouds. Chapter 4. Radiation Characteristics of the Atmosphere and the Earth's Surface. Kondratyev K. Ya., Ed., Amerind Publ. Co., New Delhi, 580 pp.

Miyake, M. and G. McBean, 1970: On the measurement of vertical humidity transport over land. Boundary-Layer Meteor., 1, 88-101.

Miyakoda, K. and J. Sirutis, 1977: Comparative integrations of global models with various parameterized processes of subgrid-scale vertical transports. Beitr. z. Phys. d. Atmos., 50, 445-447.

Monin, A. S. and A. M. Obukhov, 1954: Basic laws of turbulent mixing in the ground layer of the atmosphere. Akad. Nauk SSSR Geofiz. Inst. Tr., 151, 163-187.

_____, and A. M. Yaglom, 1966: Statistical hydromechanics, Part I: The mechanics of turbulence. Translation U.S. Dept. of Commerce, Joint Publications Research Service, No. 37, Washington, DC, 605 pp.

Nickerson, E. C. and V. E. Smiley, 1975: Surface layer and energy budget

parameterizations for mesoscale models. J. Appl. Met., 14, 197-300.

Norton, C. C., F. R. Mosher and B. Hinton, 1979: An investigation of surface albedo variation during the recent Sahel drought. J. Appl. Meteor., 18, 1252-1262.

Orvig, S. Ed., 1970: Climates of the Polar Regions. Vol. 14. World Survey of Climatology, Telseiver, 370 pp.

Paulson, C. A., 1970: The mathematical representation of wind speed and temperature profiles in the unstable atmospheric surface layer. J. Appl. Met., 9, 857-861.

Payne, R. E., 1972: Albedo of the sea surface. J. Atmos. Sci., 29, 959-970.

Penman, H. W., 1948: Natural evaporation from open water, bare soil and grass. Proceedings Royal Soc. London, Ser. A, 193, 120-145.

Pennell, W. T. and M. A. LeMone, 1974: An experimental study of turbulence structure in the fair-weather trade wind boundary layer. J. Atmos. Sci., 31, 1308-1323

Petzold, D. E., 1977: An estimation technique for snow surface albedo. Climatology Bull., 21, 1-11.

Plate, E. J., 1971: Aerodynamic characteristics of atmospheric boundary layers. AEC Critical Review Series, US Atomic Energy Commission, Div. Tech. Info., 190 pp.

Posey, J. W. and P. F. Clapp, 1964: Global distribution of normal surface albedo. Geofisica International, 4, 33-48.

Priestley, C. H. B. and R. J. Taylor, 1972: On the assessment of surface heat flux and evaporation using large scale parameters. Mon. Wea. Rev., 100, 81-92.

Reynolds, R. W., 1983: A comparison of sea surface temperature climatologies. J. Clim. Appl. Meteor., 22, 447-459.

Robock, A., 1980: The seasonal cycle of snow cover, sea ice and surface albedo. Mon. Wea. Rev., 108, 267-285.

Rotta, J., 1951: Statistische Theorie Nichthomogener Turblenz. Z. Phys., 129, 547-572.

Sawyer, J. S., 1959: The introduction of the effects of topography into methods of numerical forecasting. Quart. J. Roy. Met. Soc., 85, 31-43.

Schemm, C. E., and F. B. Lipps, 1976: Some results from a simplified model of atmospheric turbulence. J. Atmos. Sci., 33, 1021-1041.

Schutz, C., and W. L. Gates, 1972: Global climate data for surface, 800 mb, 400 mb: July. R-1029-ARPA, 180 pp. RAND, Santa Monica, CA.

_____ and _____, 1973: Global climatic data for surface 800 mb, 400 mb: April. R-1317-ARPA, 192 pp. RAND, Santa Monica, CA.

Smagorinsky, J., 1963: General circulation experiments with the primitive equations: I. The basic experiment. Mon. Wea. Rev., 91, 99-164.

_____, S. Manabe, and J. L. Holloway, 1965: Numerical results from a nine-level general circulation model of the atmosphere. Mon. Wea. Rev., 93, 727-768.

Smith, S. D. and E. G. Banke, 1975: Variation of the sea surface drag coefficient with wind speed. Quart. J. Roy. Meteor. Soc., 101, 665-673.

Tenneckes, H., 1978: Turbulent flow in two and three dimensions. Bull. Amer. Meteor., Soc., 59, 22-28.

Thornthwaite, C. W., 1948: An approach toward a rational classification of climate. Geogr. Rev., 38, 55-94.

Untersteiner, N. and F. I. Badgley, 1965: The roughness parametes z_0 of sea

ice. J. Geophys. Res., 70, 4573-4577.

Webb, E. K., 1970: Profile relationships: the log-linear range and extension to strong stability. Quart. J. Roy. Met. Soc., 96, 67-90.

Wiesnet, D. R. and M. Matson, 1979: The satellite-derived northern hemisphere snowcover record for the winter of 1977-78. Mon. Wea. Rev., 107, 928-933.

Wu, J., 1969: Wind stress and surface roughness at air-sea interrface. J. Geophys. Res., 74, 444-455.

_____, 1972: A note on surface roughness and resistance coefficient of sea ice. J. Geophys. Res., 77, 3272-3277.

Yamada, T. and G. L. Mellor, 1975: A simulation of the Wangara atmospheric boundary layer data, J. Atmos. Sci., 32, 2309-2329.

_____ and _____, 1979: A numerical simulation of the BOMEX data using a turbulence closure model coupled with ensemble cloud relations. Quart. J. Roy. Met. Soc., 105, 915-944.

Yamagishi, Y., 1980: Simulation of the air-mass transformation process using a numerical model with the detailed boundary layer parameterization. J. Met. Soc. Japan, 58, 357-377.

Yokoyama, O., M. Gamo, and S. Yamamoto, 1977: On the turbulence quantities in the atmospheric mixing layer. J. Met. Soc. Japan, 55, 182-192.